HHS Public Access

Author manuscript

Neuroimage. Author manuscript; available in PMC 2021 March 28.

Published in final edited form as:

Neuroimage. 2021 March ; 228: 117667. doi:10.1016/j.neuroimage.2020.117667.

Using non-invasive neuroimaging to enhance the care, well-being and experimental outcomes of laboratory non-human primates (monkeys)☆

M.A. Basso[a], **S. Frey**[b], **K.A. Guerriero**[c], **B. Jarraya**[d,e], **S. Kastner**[f], **K.W. Koyano**[g], **D.A. Leopold**[g], **K. Murphy**[h], **C. Poirier**[h], **W. Pope**[i], **A.C. Silva**[j], **G. Tansey**[k], **L. Uhrig**[d]

[a]Fuster Laboratory of Cognitive Neuroscience, Department of Psychiatry and Biobehavioral Sciences UCLA Los Angeles CA 90095 USA

[b]Rogue Research, Inc. Montreal, QC, Canada

[c]Washington National Primate Research Center University of Washington Seattle, WA USA

[d]Cognitive Neuroimaging Unit, INSERM, CEA, NeuroSpin center, 91191 Gif/Yvette, France

[e]Université Paris-Saclay, UVSQ, Foch hospital, Paris, France

[f]Princeton Neuroscience Institute & Department of Psychology Princeton University Princeton, NJ USA

[g]National Institute of Mental Health NIH Bethesda MD 20892 USA

[h]Biosciences Institute and Centre for Behaviour and Evolution, Faculty of Medical Sciences Newcastle University Newcastle upon Tyne NE2 4HH United Kingdom UK

[i]Department of Radiology UCLA Los Angeles, CA 90095 USA

[j]Department of Neurobiology University of Pittsburgh, Pittsburgh PA 15261 USA

[k]National Eye Institute NIH Bethesda MD 20892 USA

Abstract

Over the past 10–20 years, neuroscience witnessed an explosion in the use of non-invasive imaging methods, particularly magnetic resonance imaging (MRI), to study brain structure and function. Simultaneously, with access to MRI in many research institutions, MRI has become an indispensable tool for researchers and veterinarians to guide improvements in surgical procedures and implants and thus, experimental as well as clinical outcomes, given that access to MRI also allows for improved diagnosis and monitoring for brain disease. As part of the PRIMEatE Data Exchange, we gathered expert scientists, veterinarians, and clinicians who treat humans, to provide an overview of the use of non-invasive imaging tools, primarily MRI, to enhance experimental and welfare outcomes for laboratory non-human primates engaged in neuroscientific experiments. We aimed to provide guidance for other researchers, scientists and veterinarians in the use of this powerful imaging technology as well as to foster a larger conversation and community of scientists

☆All authors contributed equally.

and veterinarians with a shared goal of improving the well-being and experimental outcomes for laboratory animals.

1. Non-invasive imaging methods are used in experimental and clinical settings

In the neuroscientific laboratory setting there are three key reasons why non-invasive imaging is performed. The first reason is experimental. Some imaging methods allow for measurement of structure and function of large areas, if not the whole brain, of non-human primates (NHP; our focus here is on species of monkey such as rhesus and marmoset, rather than great apes). Imaging procedures can be performed while the subject is under anesthesia or while alert and performing behavioral tasks - just as typically used in human experimental neuroscience - and allowing for a deeper understanding of brain areas across primate species and their relationship to behavior. The second reason is a consideration of laboratory animal welfare. Imaging is used to refine experimental methods and techniques. For example, modern day magnetic resonance imaging (MRI) scanners are commonplace in many large research institutions and can be used to refine surgical implantation procedures as well as improve precision of experimental targets for manipulation, in much the same way that imaging is used to guide neurosurgeons who perform resections to treat people with brain tumors and epilepsy or implant deep brain stimulation electrodes to treat people with Parkinson's disease. The third reason for using imaging in the neuroscientific laboratory setting is to perform clinical assessments to prevent or treat neurological impairment and improve the well-being and health of laboratory monkeys, again, in much the same way as used in people to inform a diagnosis and guide treatments of brain disease. In what follows we review some fundamentals of two of the most common non-invasive imaging methods used in the neuroscientific laboratory setting, magnetic resonance imaging (MRI) and computerized tomography (CT). Although X-radiography is often more readily available than MRI, the lack of three-dimensional imaging makes traditional X-rays less useful in applied neuroscience. Positron emission tomography (PET) provides useful functional information, but raises issues related to handling and transport of radioactive material and radiation containment for housing animals. Ultrasonography is cost effective, but has limitations due to the bony cranial vault in adult monkeys, in which sound wave pulses do not penetrate. Therefore, we briefly review CT but focus mainly on MRI. Next, we discuss the use of MRI for surgical planning, implant design, targeting of brain areas and reconstruction of electrode penetrations as used in electrophysiological experiments. We review the use of anesthesia as well as provide some guidance based on the knowledge and experience of our veterinarian and clinician collaborators, and we review the use of MRI to detect brain pathology in laboratory monkeys. Monkey surgery and anesthesia benefit directly from the major advancements in human clinical neurosurgery and from the recent advancements in human clinical anesthesia. Finally, we briefly introduce the new area of using MRI to enhance the welfare of laboratory monkeys. For further discussion of integrating metadata with imaging data to improve well-being, we refer the reader to Poirier et al., this issue.

1.1. Computerized tomography (CT)

Computerized tomography (CT) is based on ionizing radiation in the form of X-rays. In contrast to traditional radiographs which provide a single image per each exposure, CT allows for the *X*-ray beam to move around the patient, acquiring data sets that are reconstructed to form multiple tomographic images in multiple planes with specified slice thicknesses. These image data sets can be reconstructed using various algorithms or kernels to optimize visualization of soft tissue, bone, and other important structures. CT scanning is fast, with datasets acquired on the order of seconds, which is highly advantageous in many settings, such as a compromised patient. Because CT is based on X-ray technology, the amount of energy absorbed, and ultimately image generation, depends on tissue electron density. Dense structures such as bone appear, by convention, white, whereas less dense regions such as those containing air appear black. Thus, structures are based on density relative to soft tissue: isodense (gray), hyperdense (white) and hypodense (black). Brain and surrounding tissues are composed of varying amounts of lipid, water and bone. Lipid or fat is less dense than water and, therefore, myelin with its high lipid content appears darker than gray matter, which has higher water content. Bone appears white because it is much denser than either lipid or water (Fig. 1). Additionally, there are algorithms that can be used to reconstruct image data to emphasize bone, lipid, etc., depending on the area of interest. Indeed, CT imaging is generally preferred to other forms of imaging for assessment of bone.

Different parameters govern the quality and the achievable spatial resolution of a CT examination, including, the voltage of the energy source, the acquisition time, the number of available detectors, the mode of acquisition and the beam spot size (Goldman, 2007). Typical CT scans of the monkey head are able to produce in-plane resolutions below 0.5 mm and slice thicknesses below 1 mm (Chen et al., 2017). In CT images, smaller lesions with density similar to normal tissue (isodense) can be challenging to detect. Successfully imaging the posterior fossa can be particularly difficult due to potential artifacts from surrounding hyperdense bone, obscuring brainstem and cerebellar abnormalities. CT scans, however, have high sensitivity for detecting acute hemorrhage. As blood coagulates it becomes denser, exceeding that of normal brain structures and thus appears bright, or hyperdense (Fig. 1). Associated vasogenic edema, due to abundant water content, will appear hypodense. Thus, acute parenchymal bleeds will typically appear as central hyperdensity surrounded by a ring of hypodense (dark) edema. Subarachnoid blood is also bright (hyperdense) on CT, but found within the sulci and basal cisterns rather than within the brain parenchyma. If abundant, subarachnoid blood can result in hydrocephalus, with expansion of the ventricles. Subdural blood is also extra-axial and crosses suture lines and is typically crescentic in shape. Epidural hematomas are often more focal, bi-convex or lentiform (lens shaped), and do not cross calvarial sutures. Subdural and epidural blood can both cause substantial mass effect with sulcal effacement, shifting of midline structures away from the hematoma, and narrowing or complete effacement of the basal cisterns. Substantial mass effect, often resulting in herniation of various brain structures, is associated with high levels of morbidity and mortality. With time (1–3 weeks) a hematoma diminishes in density, becoming isodense relative to brain tissue and, eventually hypodense (>3 weeks) to normal brain. Regions of hypodensity within the brain lasting longer than 1 month can result from gliosis or encephalomalacia following blood resorption.

Intravascularly injected iodine-based compounds can also be used with CT. These agents are much denser than brain tissue. Thus, iodinated contrast agents improve vascular visualization and can also be used to illustrate areas of blood-brain barrier breakdown. As some tumors and abscesses can have regions of compromised vascular integrity, iodinated contrast agents will leak into, and accumulate in, the surrounding interstitium, resulting in increased conspicuity of these lesions on post-contrast exams. Conversely, contrast injection can obscure some hyperdense abnormalities such as hemorrhage, as the increased density due to the contrast can obscure that associated with blood products.

1.2. Magnetic resonance imaging (MRI)

Magnetic resonance imaging (MRI) uses perturbation of tissue magnetization by radio waves, and thus does not rely on nucleic acid-damaging ionizing radiation utilized by CT. MRI is designed to generate images based on protons in water and, to a lesser degree, in fat. MRI has a number of advantages over CT, particularly in the ability to use multiple “pulse sequences” that generate various tissue contrast in a fundamentally different way than CT. These pulse sequences can be tailored to highlight a vast array of abnormalities, some of which are difficult, if not impossible, to detect with CT. MRI can also provide high quality structural images of the brain with submillimeter resolution and much better visualization of the distinction between white and gray matter, white matter tracts, deep nuclei and various other structures than that afforded with CT. MRI is more resistant to degradation by bone-associated artifact than CT, allowing for better visualization of posterior fossa structures. MRI is not superior to CT for all imaging applications, however; for instance, acute blood can be more difficult to image with MRI than CT, as a hematoma visualized by MRI can have a signal intensity closely matching the surrounding brain on some common pulse sequences. Nevertheless, newer pulse sequences have improved the detection of blood and blood degradation products on MRI. Bony anatomy, is poorly depicted by MRI, but as mentioned above, can be imaged with outstanding resolution and detail with CT.

MRI depends on fat and water content, and images are described in terms of signal intensity (rather than density as with CT); isointense, hyperintense, and hypointense. The most common images used in MRI are referred to as T1 and T2 weighted images, which are based on intrinsic properties of tissues and are used to generate contrast (Pooley, 2005). T1 weighted images are highly sensitive to fat content, and constructed so that areas of high lipid content such as white matter, are bright (or hyperintense). Conversely, fluid such as CSF will be dark (or hypointense) on T1-weighted images (Fig. 2, left). As with CT, injected contrast agents can be used to highlight some pathologies, particularly those that generate blood brain barrier breakdown. For MRI, contrast agents are based on the rare earth metal gadolinium, rather than iodine. Gadolinium alters the T1 properties of tissue, resulting in “T1-shortening” which is typically demonstrated as increased signal intensity in any location where gadolinium accumulates. Gadolinium has less effect on T2-weighted images and so is typically only used with T1-weighting. T2 weighted images are more sensitive to water content, thus CSF is bright, as are areas of edema. Areas of lower water content such as the brain are less intense. (Fig. 2, right). T2 signal intensity is not always the reverse of T1-weighting, however. For instance, depending on the specific pulse sequence employed, subcutaneous fat is often bright on both T1 and T2-weighted images. Similarly, extracellular

methemoglobin, found in subacute to chronic hematomas, will also be bright with both T1 and T2 weighted images.

An advantage of the MRI examination is the ability to use an array of pulse sequences to image a single body part, but with multiple forms of tissue contrast. For instance, techniques that employ “fat suppression” can reduce signal intensity in fat-rich regions, possibly leaving only the signal from underlying abnormalities, thus potentially increasing sensitivity for various pathologies. Alternatively, as many diseases manifest themselves by an increase in water content, water-sensitive sequences, typically T2-weighted, can be applied to detect subtle changes in tissue architecture indicative of underlying disease. The exact nature of the pathology can be difficult to determine as imaging findings can be non-specific. For example, infections and tumors potentially have many common imaging features. They are both space-occupying lesions with the potential for substantial mass effect, they may both generate perilesional edema demonstrated by increased peripheral T2-weighted signal intensity, and may both enhance with gadolinium contrast agents, secondary to break-down of the blood brain barrier (Fig. 3). One pulse sequence that may be beneficial in distinguishing these two entities is diffusion-weighted images, which are bright in regions where the molecular motion of water is reduced. This can occur within abscesses but is rarely evident in tumors. Thus, although not necessarily a specific imaging marker of abscess, there is a high positive predictive value for diffusion signal abnormality in the appropriate clinical setting.

1.3. Using MRI for pre-surgical planning

In clinical human neurosurgery, MRI is routinely used to plan the surgical approach. Pre-surgical planning in NHP neuroscientific experiments using MRI has increased significantly over the last two decades. It is now routine in many laboratories for MRI to be performed prior to invasive procedures to improve and optimize targeting accuracy for experiments involving procedures such as electrode insertion or compound injections. Using imaging technology to refine experimental procedures and reduce the number of animals used in research where possible, helps to fulfil our ethical responsibilities as laboratory animal users (Russell and Burch, 1959).

Traditionally, before the routine use of MRI, the stereotaxic frame - a version of which was first introduced by Horsley and Clarke in 1908 - was used as a tool for targeting brain regions in the NHP along with a 3D coordinate system, anterior-posterior; medial-lateral and dorsal-ventral. Using the stereotaxic method, neurosurgical planning relied on 3D stereotaxic coordinates derived from paper atlases representing cytoarchitecture analyzed from a single subject taken from histological brain slices in the interaural plane (Paxinos et al., 2000; Paxinos et al., 2008; Saleem and Logothetis, 2007; Snider and Lee, 1961; Szabo and Cowan, 1984). Even in combination with early MRI, atlases aided target localization when imaging technology had insufficient resolution. Although digital atlases with improvements in nonlinear registration to specific NHP brains have been realized more recently (Frey et al., 2011; Reveley et al., 2017), these digital data still refer back to individual anatomical boundaries. The boundaries are determined from a very small number of animals and therefore the resulting coordinate systems are not always reliable.

Ventriculoradiography is another traditional method used to provide anatomical information. Ventriculoradiography requires surgical infiltration of iodine-based compounds into the foramen of Munro (Crawford et al., 1989; Gearing and Terasawa, 1988). In experienced hands, this approach added valuable information for the neurosurgical approach, and was successfully used to place indwelling electrodes for short-term studies. However, ventriculography is an invasive and risky procedure that is not often used in clinical stereotaxy. Moreover, ventriculographic guidance is indirect because brain targets are not visualized.

With the introduction of MRI-compatible stereotaxic frames, surgical planning in NHPs has become easier (Alvarez-Royo et al., 1991; Maciunas and Galloway, 1989; Saunders et al., 1990), although issues with getting the animal into the exact same frame position for surgery as during the MRI scan is impossible and can lead to errors in registration (Dubowitz and Scadeng, 2011). This is a problem of repeat fixation for stereotactic procedures. The targeting errors may only be a few millimeters, but when targeting small nuclei, small errors have large impacts on the accuracy of the procedure, as the mouth piece position induces further differences in final head positioning. Furthermore, limitations with the size of the animal and placement of radio-frequency (RF) coils around the frame to get adequate signal from the NHP brain can make scanning with a frame problematic. To improve on surgical targeting when using a stereotaxic frame in the MRI, the animal should be transported immediately to the surgical suite after the scan so that the reference frame is kept in place to prevent positioning error. This, however, is not feasible in many institutions, not to mention that errors compound and time is lost when complicated equations need to be calculated for trajectories to target areas that are not perpendicular to the skull or to the imaging plane. High definition video cameras or even lasers are starting to be used in human neurosurgery to co-register patients in the operating room to the MR images by scanning facial or head features and superimposing these onto existing reconstructions of the same areas; a type of non-contact registration with distance measuring (Willems et al., 2001; Schlaier and Brawanski, 2002; Raabe et al., 2002; Shamir et al., 2009). Although this works fairly well for large human heads and faces, the resolution is not high enough yet, for use in the smaller monkey. In addition, updating MR images to an animal’s brain in surgery may eventually be possible with the use of new imaging co-registration technologies. For instance, although somewhat experimental, some human neurosurgeons are using hand-held ultrasound technology co-registered to the MRI patient data to update the MR images in real-time (Park et al., 2017). This is extremely useful when brain shift occurs. These hand-held ultrasound probes are becoming smaller, however, a large craniotomy is still required as ultrasound attenuates through bone and thus, this approach remains experimental.

As surgical planning and imaging continue to evolve, accuracy and flexibility using a frameless image-guided system for NHP targeting is seen as an advantage to rigid frame-based systems. This technology is also called neuronavigation. Neuronavigation was developed successfully in human clinical neurosurgery and became a routine equipment in hospital operating rooms (Enchev, 2009). Neuronavigation systems, which use the MRI scan and fiducial markers that are placed on the NHP prior to imaging, allow the researcher to plan target locations and trajectories effortlessly, only to access these structures at a later date in the operating suite with real-time precision (Frey et al., 2004). Neuronavigation

assistance improves guidance and localization during craniotomy procedures, and ultimately improves patient outcome (Enchev, 2009). More recently, use of intraoperative MRI for targeting has also been used for accurate target positioning in the NHP. In this case, preliminary anatomical scans are acquired and targets can be reached using MRI compatible devices while inside the bore of the scanner. New scans are acquired to check for targeting accuracy, and modifications can be made immediately on the bed of the MRI to correct targets or trajectories, something that is critical especially if brain shift occurs after a craniotomy. However, working closely within the confines of the MRI field as well as using MRI compatible devices and tools, not to mention the high costs associated with this type of surgery, makes this type of surgery unattainable for most NHP researchers (Emborg et al., 2010). Although individual anatomical differences exist between animals, there is still a degree of certainty when it comes to structures based on cytoarchi-tectonic boundaries between sulcal and gyral patterns in the NHP brain (Amiez et al., 2019). In this regard, it is advantageous for researchers in the presurgical planning phase to be able to visualize and accurately target regions of interest using MRI images in their research animals prior to surgery. More importantly, it is extremely beneficial to have computer software that can accept the relevant imaging data, including atlases, and allow for recreations of implants or simulations of devices down to deep brain areas (Fig. 4) (Frey et al., 2004; Ohayon and Tsao, 2012).

That same software needs to be able to guide the researcher in placing the implants or devices into the correct location during surgery as well. Both task-based and resting-state blood-oxygenation-level-dependent (BOLD) fMRI can also be used as powerful tools when planning for more invasive experimentation in the NHP brain (Fig. 5). Whether acquired in an awake or anesthetized state, functional imaging data can be superimposed on anatomical data to decipher where in the brain additional experimentation needs to take place when characterizing cortical areas involved in cognitive or perceptual processing (Goense and Logothetis, 2008; Kayser et al., 2009; Maier et al., 2008; Wang et al., 2013; Wilson et al., 2016).

A helpful addition to surgical planning for neuroscientific experiments in NHPs is to include vascular imaging to avoid major blood vessels when penetrating the brain. Although most clinical MRI machines are set up with preloaded angiography sequences for human, many of these sequences are not ideal for smaller brains (monkey brains are about 25–30% in size relative to human brains). Alternatively, injecting the anesthetized animal with Gadolinium contrast medium (10–12 mg/kg) leads to a hyperintensity in the anatomical images and highlights the major vessels of the brain sufficiently.

Finally, with the use of radio-frequency (RF) coils for NHPs in ultra-high field MRI scanners (Gao et al., 2020), or RF coils that are able to produce similar contrast and signal-to-noise results in lower field MRI machines, the results will ultimately lead to better visualization and therefore better surgical planning for NHPs in the future. Ultra-high field MRI, and the eventual addition of contrast agents, could enhance the visualization of deep seated nuclei of basal ganglia in macaques as an example (Tani et al., 2011). Although there are still many limitations to overcome with these techniques, the increase in resolution not only helps pre-surgical planning but will also help targeting in the NHP brain. Higher field

MRIs also carry higher risks of distortion that should be accounted for in surgical targeting (Poulen et al., 2020).

1.4. Using MRI to design custom implants

The majority of neuroscientists who study the structure and function of the NHP brain, especially electrophysiologists and neuroimaging experts, rely on implanted devices on the skull. These implants are used to eep the head stable, or may have chambers attached that allow access to the brain, so that neuronal data from electrodes in underlying brain regions can be collected. MRI and CT imaging can be used to target regions of interest successfully. However, creating an implant and locating the exact position where these implants need to be placed over the brain can be difficult if custom software is not used (Chen et al., 2017; Johnston et al., 2016; McAndrew et al., 2012; Mulliken et al., 2015; Ohayon and Tsao, 2012). Although stainless steel implants along with bone cement are still used in some laboratories, titanium has been the material of choice for many implanted devices over the years as it is MRI safe (titanium is non-ferromagnetic) and adheres well to bone through osseointegration (Adams et al., 2007; Adams et al., 2011; McAndrew et al., 2012; Overton et al., 2017). Unfortunately, titanium implants and screws also produce large signal or image artifact and distortion in MRI that can occlude the underlying brain anatomy (Fig. 6). Moreover, in spite of the relative safety of titanium (it is non-ferromagnetic), titanium posts render fMRI impossible because the echo planar imaging (EPI) signal is much more sensitive to the magnetic distortions caused by the titanium.

As an alternative to titanium, plastic implants, such as polyetheretherketone (PEEK) coupled with ceramic screws can be used, as they do not have imaging artifact limitations. The thermoplastic materials, as well as the ceramic screws that attach the implant to the bone, are extremely rigid, produce no unwanted signal artifact or distortion in the MRI and are biologically inert. Thus, PEEK implants are both MRI safe and MRI compatible. However, since PEEK is biologically inert, it implies that PEEK does not bind well to tissue or bone. As a work around, bone cement or acrylic can be placed on the implant as a supportive function, but most of these products are exothermic and potentially cytotoxic, which can be detrimental to the bone and the surrounding skin margins, requiring special care when using these products (Dahl et al., 1994; Dunne and Orr, 2002).

Bone cement is also inert, and thus the skin and underlying fascia do not interact and grow on this material. Furthermore, the skin/acrylic interface is a potential source of irritation and infection, as it is impossible to keep the animal from picking and scratching at the margin. Granulation tissue can also grow under the acrylic and the bone, presenting a site where possible infection can set in (Adams et al., 2011; Mulliken et al., 2015); this can not only compromise the stability of the implant, but also the health of the animal, as it is difficult to treat and clean. In addition, having the bone cement in direct contact with the skull can lead to the creation of porous bone, and since the bone cement is adhering to screws holding the implant in place, this can jeopardize the stability of the implant. Finally, the use of bone cement increases the height and circumference of the total implant surface. The former has direct consequences for MRI studies because the bone cement can interfere with the placement of the RF coils around the head of the subject. The increased implant area

consequently reduces the surface area of the healthy normal skull. Thus, bone cement not only creates large implant surfaces that are visually unappealing, but can lead to greater skin retraction and can make it difficult to suture the remaining skin if an implant is explanted.

Recent advances have been made with respect to acrylic-free titanium (Adams et al., 2011; Chen et al., 2017) and PEEK implants, i.e., that both materials can be custom shaped to the bone (Blonde et al., 2018; Mulliken et al., 2015) yet due to several of the challenges mentioned above, concessions still need to be made. To accelerate bone adhesion as well as skin retention with non-acrylic implants, an orthopedic coating is sometimes applied to accelerate osseointegration of titanium and PEEK implants such as hydroxyapatite; a mineral form of calcium known for its adhesion and osseointegration properties. For neuroimaging researchers, especially those who would want to minimize signal artifact by using PEEK, hydroxyapatite is a good addition. Unfortunately, most plastic adherence research (Depprich et al., 2008; Kurtz and Devine, 2007; Masoud et al., 1986) in orthopedics uses large bones (e.g., femur). The types of implants needed in NHP research are significantly different because they are always on the skull, which is quite thin (2–4 mm), and the implant/bone bond must withstand the weight of the animal during head restraint and other forces the implant may incur. Thus, the adherence characteristics of an implant in long bones may differ significantly from implants that are always located externally on a thin NHP skull. Ironically, in most cases hydroxyapatite can only be applied to an implant surface if a thin layer of titanium (> 50 μm) is first applied as a rough matrix (Stübinger et al., 2016). Fortunately, this thin layer does not create significant artifact or distortion with MR imaging and more recently has proven successful with PEEK implants, especially when repeated neuroimaging is required (Ortiz-Rios et al., 2018).

Custom implants in NHP that are form fitting and make contact with bone adhere to the skull better and last longer. Specifically, recording chambers that have a better fit with the bone are more hermetically sealed and help to avoid infection. Finally, with the use of engineering software, stress testing of custom implants (e.g. SolidWorks, USA) can be performed to ensure structural stability of the custom shapes before they are manufactured (Fig. 7).

Custom implants can be created using existing MRI and/or CT data and generating three-dimensional (3D) reconstructions of the skull. Computer-Aided Design (CAD) files are introduced into a given software (Chen et al., 2017; Johnston et al., 2016; McAndrew et al., 2012; Mulliken et al., 2015; Ohayon and Tsao, 2012) and the intersection of the CAD file with the reconstructed bone surface of the animal creates a new CAD file. This ensures that the implant sits precisely over the bone area of interest; making contact with the bone surface and forming a better seal. These CAD files can then be sent to a high-resolution 3D printer or accurately manufactured using 5-axis CNC machines with high quality plastic materials (Fig. 8).

1.5. Using MRI to localize electrode penetrations

Although there is an increasingly large group of neuroscientists performing imaging experiments in NHPs as desribed below in more detail, traditionally the NHP model is used to combine sophisticated behavioral experiments with neurophysiological recordings from

brain areas. In the realm of neurophysiology, structural MRI has become indipensible for many neuroscientists to assess electrode position and placement. Single-unit recording using microelectrodes can collect responses of individual neurons with high temporal resolution, and precise identification of the location of the recorded neurophysiological responses reveal functional architectures of the brain Mountcastle (1997). The widely accepted method for localization is marking of the recording sites with electrolytic micro-lesions, which can be subsequently detected by *postmortem* histology (Hubel and Wiesel, 1962). This gold-standard method precisely localizes the recording sites with detailed histological information of surrounding brain tissue; however, electrolytic mark recovery requires euthanizing the animal for histological processing. In addition, since closely marked multiple micro-lesions are difficult to identify, the number of detectable recording sites within a local volume is limited. Therefore, the micro-lesion method typically requires euthanasia of a greater number of animals to collect sufficient data. This *postmortem* procedure is sufficient for experiments using acute preparations, but it is not easy to apply to chronic experiments using behaving NHPs that often continues for months or years. In chronic recordings, the location of recording sites used to remain unknown until the completion of all the *in vivo* experiments. Recent advancements of *in vivo* neuroimaging techniques overcome this problem and can also be applied to chronic recordings which have revealed fundamental functions of the NHP brain (Buffalo et al., 2019).

As mentioned earlier, more than a century ago, a stereotaxic targeting procedure was developed (Horsely and Clarke, 1908). The recording area was estimated from the coordinates that were derived from a standardized atlas. This *in vivo* method is easy and has been used for estimating recording areas, but also suffers from errors due to significant variation of the shape/size of the NHP brain across individuals (Percheron et al., 1972; Wagman et al., 1975). Development of the MRI technique drastically improved the precision of the stereotaxic estimation by its ability to visualize soft brain tissue of each subject (Alvarez-Royo et al., 1991; Asahi et al., 2003; Rebert et al., 1991; Saunders et al., 1990; Walbridge et al., 2006). More recently, MRI has been used to confirm location of recording chambers to better estimate actual recording sites that is specific to the implanted chambers (Daye et al., 2013; Kalwani et al., 2009; Ohayon and Tsao, 2012; Talbot et al., 2012). When chambers are made from MRI-compatible plastic materials that cannot be directly visualized by MRI, a liquid-filled recording grid can be placed inside of the chamber during the scan (Fig. 11). Based on the location of the grid holes, it is possible to determine which grid holes correspond to the target recording area. This straightforward method requires just one post-surgical scan and is now routinely used in many laboratories to determine recording areas.

To map recording sites within fine brain architecture less than a millimeter, such as the columnar organization or cortical layers, it is adequate to localize recording sites for each electrode penetration. When recording from deep areas of the brain, small variations of trajectory angles during the penetration leads to larger errors at the recording sites. For example, a one-degree difference at the top of a 20 mm-height chamber causes a 1 mm difference at 40 mm depth of the brain. Multiple factors potentially cause small deviations of the penetration angle, including electrode holding by the microdrive, small slipping during penetration of dura mater, or slight curvature of electrode during the penetration. When the targeting error is less than 1 mm, it does not matter in most cases for determining recording

regions, such as whether recording from primary or secondary visual cortices. However, to study finer brain architectures such as columnar organization or cortical layers, it is necessary to localize recording sites precisely for each penetration. Neuroimaging techniques of different modalities can visualize inserted probes *in vivo* (Fig. 12), including ultrasonography (Collier et al., 1980; Glimcher et al., 2001; Tokuno et al., 2000), X-ray imaging (Aggleton and Passingham, 1981; Cox et al., 2008; Nahm et al., 1994), CT scanning (Premereur et al., 2020) and MRI (Koyano et al., 2016; Matsui et al., 2007; Tammer et al., 2006). Each method has its own advantages and disadvantages. Ultrasonography can visualize the tissue with the inserted electrode in real-time, and monitor when the probe is inserted and how surrounding tissue is deformed and moved back to the original position. The real-time visualization of electrode penetration can reduce the risk of hitting blood vessels and potentially prevent iatrogenic stroke, but due to the lack of soft tissue contrast and the restricted field of view, the use of ultrasonography, as mentioned above, is currently limited. Radiographic methods, both X-ray imaging and CT scanning, can visualize intracranial probes with clear contrast and extremely high-resolution of tens of micrometers. The scanning time is just a few seconds (X-ray) to a minute (CT), which is a great advantage for daily use. Furthermore, with appropriate shielding, X-ray can be taken at the recording booth without anesthetizing animals after every electrophysiology session. The limitations of the radiographic methods are, primarily, the lack of soft tissue contrast, which needs to be complemented by other modalities, most typically with MRI. Both the MRI and radiographic images can be co-registered with referring skull landmarks or fiducial marks implanted on the skull. For chronic experiments, it is often needed to take MRI images periodically since skull and brain tissue slowly change their size and shape over years.

MRI can be used to localize recording sites directly, and can visualize the brain tissue with high tissue contrast at a resolution of a hundred micrometers. The difficulty of MRI usage in localization of recording sites is the magnetic susceptibility artifact caused by metal, which is a common material of electrodes. When it comes to imaging implanted device with MRI, it is key to check for the safety of the procedure. Many implanted metallic systems (leads/connectors) are not compatible with MRI or not safe at all fields (Erhardt et al., 2018). It should be noted that imaging the implanted brain with MRI could lead to severe adverse events such as brain hemorrhage in patients with intracranial electrodes (Henderson et al., 2005). There are two MRI-based methods: 1) direct visualization of inserted electrode (Matsui et al., 2007; Tammer et al., 2006), and 2) detecting marks deposited at the recording sites (Fung et al., 1998; Koyano et al., 2011; Pezaris and Dubowitz, 1999; Premereur et al., 2020). The first method is direct visualization of inserted metal electrode which is depicted as a dark shadow along the electrode in the images of MRI (Fig. 12 B and 13 A, B). The shadow is larger than the electrode, because the metal core of the electrode has different magnetic susceptibility from the surrounding tissue. This susceptibility difference causes geometrical distortion and signal loss due to intravoxel phase dispersion (the so-called T2* effect), resulting in the shadow of the electrode. A previous study showed that the electrode shadow can be used to enhance the detectability of electrode tip, and under specific geometric conditions, the electrode tip can be localized precisely *in vivo* (Matsui et al., 2007). This method has the advantage of localizing electrode tips together with surrounding brain tissue at high contrast and high spatial resolution. However, the method also requires

frequent access to an MRI scanner, which is not a practical choice for every laboratory. The second MRI-based method is detection of marks that are left in the brain (Figure 13 C, D) (Fung et al., 1998; Koyano et al., 2011; Pezaris and Dubowitz, 1999; Premereur et al., 2020). This method first creates a small metal deposit during the penetration by passing electrolytic current from the tip of the metal electrode. Because the created deposit mark contains metals of the electrode, it causes a local susceptibility artifact, and can be detected by MRI as a small dark spot. This method does not require MRI scanning during each penetration, and multiple deposited marks can be detected at a single scan, making it easier to use in many laboratories. A potential drawback of this marking method is the limitation of repeated use in a small region, since it might cause damage of tissue that is needed for the study, and closely spaced marks are difficult to distinguish from each other. The metal deposit can be also used in combination with other imaging methods, and utilized as a within-brain fiducial mark to co-register with other image modalities or histological sections. A previous study combined these two MRI-based localization methods and histology, and revealed functional differences of adjacent cortical layers (Koyano et al., 2016).

1.6. Targeting brain regions - diffusion MRI (dMRI)

Whereas structural MRI aids the identification of brain regions within gray matter as well as subcortical nuclei that have a great density of neurons, diffusion MRI (dMRI) can define the structural connectivity, i.e. the white matter fiber tracts between cortical regions and subcortical structures. Diffusion MRI utilizes the fact that the diffusivity of water molecules is stronger following the direction of fiber passages than other directions (e.g. perpendicular to them). The method is constrained by the number of directions that can be traced in a given voxel and by the size of the voxel. Together, these constraints make diffusion MRI an *in vivo* anatomical tracing method with moderate resolution. However, major fiber bundles running anterior-to-posterior and connecting frontal with parietal and temporal cortex can be readily identified (Assaf et al., 2019) as well as the connectivity of major subcortical structures such as thalamic nuclei with their cortical projection targets (Arcaro et al., 2015b; Saalmann et al., 2012).

The accuracy of identifying fiber tracts using diffusion MRI is compromised particularly by head motion and the amount of data that can be acquired in a given session. These parameters have limited the success of dMRI in human applications. In NHP research, these parameters can be controlled much more favorably. First, dMRI is typically conducted while animals are sedated or anesthetized, thus eliminating head motion as a noise variable and permitting the acquisition of larger data sets per session. Second, by using an MRI-compatible stereotaxic apparatus, the animal’s brain can be aligned precisely from session-to-session, and data can be concatenated across sessions. Thus, large data sets with fewer artifacts can be readily acquired in NHPs. Ideally, a dMRI data set should be acquired before performing any head implantations, since implants can cause considerable artifacts in diffusion images. As for practical examples, tract tracing results from dMRI can be particularly helpful in reconstructing interconnected sites of large-scale networks to identify targets for simultaneous large-scale recordings (Saalmann et al., 2012) or to identify the connectivity of a brain region under investigation.

1.7. Targeting brain regions - task-based functional MRI (fMRI)

The mapping of functional brain regions using BOLD contrast in fMRI experiments has become the most widely used technique, particularly in human neuroscience (Ogawa et al., 1990). BOLD-fMRI provides whole-brain coverage with sub-millimeter spatial resolution, excellent contrast-to-noise ratio, and relative ease of implementation. Like positron-emission tomography (PET) and diffuse optical tomography (which uses near-infrared spectroscopy to generate 3D images), BOLD-fMRI relies on neurovascular coupling - a tight relationship between changes in neural activity and local cerebral blood flow (CBF), volume (CBV), and oxygen consumption ($CMRO_2$) (Gauthier and Fan, 2019). Brain stimulation is achieved by using sensory, motor, or cognitive tasks that cause regional increases in neural activity. These translate into local increases in CBF that exceed the increases in $CMRO_2$, leading to increases in oxygenation levels in the venous vasculature that produce a higher BOLD fMRI signal measured at activation, relative to baseline. Because NHPs are phylogenetically close to humans, they have been the premier model used in studies of visual perception and attention, sensorimotor and cognitive brain processes. The first fMRI experiments in anesthetized or awake behaving monkeys were performed in the late 1990s, using either visual (Dubowitz et al., 1998; Logothetis et al., 1999; Stefanacci et al., 1998) or somatosensory stimulation (Disbrow et al., 1999). Since then, task-based fMRI has been routinely employed to understand the functional and anatomical organization of the NHP brain. For important reviews, see (Alkemade et al., 2015; Duong, 2010; Janssen et al., 2018; Logothetis, 2003a; Nakahara et al., 2007; Orban, 2016; Orban et al., 2004; Seidlitz et al., 2018; Silva, 2017; Tootell et al., 2003; Tsao, 2014; Tsao and Livingstone, 2008).

1.8. Targeting brain regions - resting state functional MRI

A complementary approach to determine interconnected network nodes is the use of resting state functional MRI (rsfMRI). Functional interactions between distributed brain areas within specific neural networks give rise to coherent patterns of hemodynamic signals, measured as BOLD activity. Covariant relations of spontaneous BOLD signals in the resting state have been reported in humans (Arcaro et al., 2015a; Biswal et al., 1995; Fox et al., 2009; Power et al., 2011; Sporns and Honey, 2013) and awake NHPs (Belcher et al., 2016; Ghahremani et al., 2017; Hori et al., 2020a; Leopold et al., 2003; Liu et al., 2013; Logothetis, 2003b; Silva, 2017; Wang et al., 2012) as well as in anesthetized NHPs (Hori et al., 2020a, b; Hutchison et al., 2012; Hutchison et al., 2013; Mantini et al., 2012a; Vincent et al., 2007; Wu et al., 2016; Wu et al., 2017; Zhang et al., 2019). These studies have revealed that specialized cognitive and sensory networks retain their basic functional connectivity, even when not specifically engaged in task-relevant operations. For example, visual field locations that correspond in eccentricity correlate stronger than non-corresponding locations (Arcaro et al., 2015a), indicating that the visual field map structure is preserved regardless of perceptual state. Similarly, networks dedicated to memory, attention and eye movements, motor functions and many sensory and cognitive domains can be readily determined in individual subjects. Resting state fMRI studies have proven useful for characterizing network architectures and for exploring alterations in neurological and psychiatric disorders as well as in development (Dosenbach et al., 2010; Sheffield and Barch, 2016). In the context of research using monkeys, it can be useful to obtain a rsfMRI data set as a routine to guide later reconstruction of the functional connectivity and network architecture of

experimental sites. Such a data set can be acquired in awake or anesthetized animals. However, it should be noted that the awake state will require head fixation and training of the NHP and acclimating the animals to sit in an MRI-compatible primate chair, either vertically for some MRI systems, or more commonly in the 'sphinx' position, for the more common horizontal MRI scanner bores. The anesthetized state may appear more straightforward, but is complicated by the low tolerance of the BOLD signal to anesthetics such as isoflurane, therefore requiring specialized anesthesia protocols.

Although there is an effort to perform imaging experiments in NHPs while alert and even behaving as discussed more below, a key aspect of obtaining MR images from NHPs depends upon the use of anesthesia. In what follows, we first discuss the influence and impact of anesthesia on imaging modalities as well as provide example protocols that are used in our facilities. Next, we compare advantages and disadvantages of both alert and anesthetized imaging procedures.

1.9. Task-based and resting-state fMRI experiments: anesthesia

Anesthetic agents represent a heterogeneous group of pharmacological agents by targeting specific receptors in the central nervous system (Franks, 2008). Anesthetics induce a reproducible and reversible loss of consciousness and memory with still an incomplete understanding of how binding to receptors leads to sedation and loss of consciousness and memory. The use of anesthetics offers important advantages of ensuring compliance, minimizing movement, and alleviating stress, which are all essential factors when imaging NHPs. Task-based (eg., sensory stimulation) and resting-state fMRI under anesthesia allows scanning NHP without the need for long behavioral training steps, and could extend its access to a wider community of neuroscience laboratories. There are however, several challenges that face the practical application of routine fMRI studies in monkeys under anesthesia. Imaging studies of brain function require a careful balance between achieving proper sedation of the animal while minimizing the interference of the anesthetic agent on brain function. Anesthetic agents affect cerebral blood oxygenation (Uhrig et al., 2014a), potentially interfere with the BOLD/fMRI signal dramatically (Hyder et al., 2002; Maandag et al., 2007) and ultimately question the interpretation of the statistical maps derived from the imaging procedure. The fMRI signal is directly influenced by physiological parameters such as body temperature (Ogawa et al., 1990) and expired CO_2 ($EtCO_2$) (Sicard and Duong, 2005). An increase of arterial blood CO_2 induces cerebral vasodilation and an increase of cerebral blood flow, leading to an increase of the baseline BOLD signal Sicard and Duong (2005). The stimuli-evoked BOLD response decreases with hypercapnia Sicard and Duong (2005). In rats, an increase in blood pressure increases the BOLD signal (Wang et al., 2006). For NHPs with intact autoregulation and without any brain lesion, as for humans (Drummond, 2019), it likely takes a significant change in mean arterial pressure before any changes in CBF are observed, which consequently affect the BOLD signal. We suggest maintaining physiological parameters in the normal range for monkeys as defined by Logothetis and colleagues (Logothetis et al., 1999) during maintenance of anesthesia; heart rate: 63–180 beats/min; SpO_2 : 89–100%; systolic blood pressure: 56–150 mmHg, diastolic blood pressure: 30–124 mmHg; respiration rate: 23–32/min, EtCO2: 36–43 mmHg and temperature: 37–38.5 °C). We note however, that high doses of isoflurane (2%) lead to

abnormal CBF increases in macaque monkeys (Li et al., 2014). Body temperature is another critical parameter for the fMRI signal (Ogawa et al., 1990). An increase in body temperature is associated with a decrease in the BOLD contrast, which could be explained by the decreased oxygen affinity of hemoglobin and the increased amount of deoxyhemoglobin. Thus, it is of high importance to keep body temperature stable during fMRI studies and avoiding hypothermia that occurs rapidly under sedation. Anesthesia for fMRI needs expertise for the sake of reproducibility and robustness to achieve stable anesthesia and to monitor accurately the depth of anesthesia during anesthesia fMRI experiments. This is particularly important for the consistency of anesthesia across sessions and individual animals. Behavioral evaluation of arousal could be performed to monitor the depth of anesthesia by means of adapted sedation scale (Uhrig et al., 2016). However, these scales are difficult to pursue during the MRI sessions as the animal is difficult to access once inside the scanner bore. There are reports of simultaneous EEG-fMRI modalities in macaques but the use of EEG inside the MRI suite is still not routine in NHPs (Fig. 9) (Uhrig et al., 2016; Vincent et al., 2007).

The volatile anesthetics isoflurane (Hori et al., 2020a; Hutchison et al., 2014; Li et al., 2013; Li et al., 2014; Li and Zhang, 2017; Vincent et al., 2007; Wu et al., 2016; Zhang et al., 2019) and sevoflurane (Pró-Sistiaga et al., 2012; Uhrig et al., 2018) are attractive in that they can be safely administered to provide satisfactory depth of anesthesia, with relatively quick onset of action, and smooth recovery of the animals upon withdrawal of the anesthetic. Using ultra-high field MRI, it has been demonstrated that the T2*-oxygenation-ratio varied as a function of the anesthetic agent, showing a higher T2*-oxygenation-ratio under volatile anesthetics (isoflurane, sevoflurane) compared to intravenous anesthetics (propofol, ketamine, midazolam) (Uhrig et al., 2014a). However, while both anesthetics are safe to use in repetitive studies in the same animal, they suppress neuronal activity and decrease functional brain connectivity (Ranft et al., 2016; Standage et al., 2020; Wu et al., 2016) in a dose-dependent manner (Hutchison et al., 2014; Li et al., 2013; Lv et al., 2016). In particular, both high and low concentrations of isoflurane were found to profoundly affect vertebral blood flow, cerebrovascular tone, and cerebrovascular reactivity (Li et al., 2013; Li et al., 2014; Li and Zhang, 2017) with complex interactions. For example, Li and colleagues found that regional levels of cerebral blood flow in the macaque brain correlated linearly with increasing concentrations of isoflurane, with abnormal increases noted at the high dose of 2.0% isoflurane concentration (Li et al., 2014), whereas prolonged exposures to low (1.0%) concentrations leads to global reductions in vertebral blood flow and resting-state networks such as the default-mode network Li and Zhang (2017). The investigation of the effects of anesthesia on brain function is an active subject of research in rodents (Bukhari et al., 2017; Bukhari et al., 2018; Grandjean et al., 2014; Uhrig et al., 2014a), NHPs (Barttfeld et al., 2015; Hori et al., 2020a; Hutchison et al., 2014; Li et al., 2014; Liu et al., 2013; Uhrig et al., 2016; Uhrig et al., 2018) and humans (Golkowski et al., 2019; Hudetz, 2012; Liu et al., 2017).

The choice of the anesthetic agent is key for task-based and resting-state fMRI experiments. As an alternative to inhalant anesthetics, injectable agents such as ketamine or propofol, and adjuncts such as medetomidine are attractive in providing a satisfactory depth of anesthesia, with relatively quick onset of action, and reversible smooth recovery of the animals

(Bertrand et al., 2016; Bertrand et al., 2017; Bola et al., 2018; Fahlman et al., 2006; Hess et al., 2012; Krzemi ń ski et al., 2017; Lee et al., 2010; Liu et al., 2015b; Lugo-Roman et al., 2010; Pulley et al., 2004; Settle et al., 2010; Sun et al., 2003; Young et al., 1999). Propofol is an injectable anesthetic with a rapid mechanism of action that is widely used in humans (Amico et al., 2014; Boveroux et al., 2010; Golkowski et al., 2019; Gómez et al., 2013; Huang et al., 2018; Hudetz, 2012; Hudetz et al., 2015; Jordan et al., 2013; Lee et al., 2013; Li et al., 2019), and increasingly used in fMRI experiments in animal models, including rodents (Grandjean et al., 2014) and NHPs (Barttfeld et al., 2015; Bola et al., 2018; Ishizawa et al., 2016; Krzemi ń ski et al., 2017; Uhrig et al., 2016; Uhrig et al., 2018). The depth of anesthesia under propofol, based on a both behavioral testing with a clinical sedation scale (Uhrig et al., 2016) and/or EEG (Uhrig et al., 2016) can be readily adjusted by varying the rate of infusion, and the animals quickly recover at the end of the experiment, thus facilitating longitudinal studies. Although it is challenging to combine EEG and fMRI, more and more EEG caps are available for NHPs and can connect to the main EEG amplifier that is also used for humans (Uhrig et al., 2016).

In the case of propofol, target controlled infusion technology (TCI) using a dedicated model called ‘Paedfusor’ pharmacokinetic model can be used (Barttfeld et al., 2015; Uhrig et al., 2016), adapting the administrated dose of propofol over time. The TCI infusion system constantly adjusts the infusion rate to maintain the targeted plasma concentration of propofol. This method is more and more used in human clinical anesthesiology. Another agent proposed as suitable for repetitive studies is the α_2-adrenoreceptor agonist medetomidine hydrochloride (Bertrand et al., 2016; Bertrand et al., 2017; Bola et al., 2018; Fahlman et al., 2006; Hess et al., 2012; Krzemi ń ski et al., 2017; Lee et al., 2010; Liu et al., 2015b; Lugo-Roman et al., 2010; Pulley et al., 2004; Settle et al., 2010; Sun et al., 2003), which allows the measurement of robust electrocorticography (ECoG) resting state signal fluctuations in the brain of NHPs (Liu et al., 2015b). The application of atipamezole hydrochloride quickly reverses the sedative and analgesic effects of medetomidine. However, some limitations of repeated and prolonged exposures to medetomidine include a gradual rise in blood pressure and heart rate, lower SpO_2 values, altered serum biochemistry, and a more difficult control of the plane of anesthesia due to the development of tolerance effects (Lee et al., 2010; Lugo-Roman et al., 2010; Sun et al., 2003).

1.10. Task-based and resting-state fMRI experiments: conscious, awake subjects and comparison with anesthesia

On the one hand, the use of anesthesia for MRI and fMRI studies has the advantage of effectively ensuring compliance and of minimizing stress. On the other hand, the many effects of anesthesia on brain function and physiology introduces significant confounds to the interpretability and applicability of the obtained data. Further, anesthetized animals cannot engage in behavioral experiments, which constitutes a significant detraction for the use of NHPs as experimental models of aspects of human brain function. Furthermore, having the capability to collect data from awake animals increases the proper translation of experimental conditions, as human subjects are studied in the conscious, awake condition. The use of conscious, awake NHPs in neuroimaging experiments is becoming increasingly popular, as exemplified by numerous studies (Andersen et al., 2002; Belcher et al., 2016;

Chen et al., 2012; Goense and Logothetis, 2008; Grinvald et al., 1991; Hori et al., 2020a; Hung et al., 2015; Liu et al., 2013; Mantini et al., 2012b; Nelissen and Vanduffel, 2011; Orban et al., 2004; Santisakultarm et al., 2016; Schaeffer et al., 2019; Sharma et al., 2019; Silva, 2017; Tootell et al., 2003; Tsukada et al., 2000; Vanduffel et al., 2001; Yamada et al., 2016). Much work has been done to compare functional data obtained in awake versus anesthetized conditions (Barttfeld et al., 2015; Krzeminski et al., 2017; Liu et al., 2013; Liu et al., 2015a; Uhrig et al., 2016; Uhrig et al., 2018). In fact, anesthesia can be used as a model for studying reversible loss of consciousness and its underlying neural mechanisms. The spatial distribution of the effects of anesthetics in the brain is not uniform, as some regions, such as the precuneus, posterior cingulate gyrus, prefrontal dorsolateral cortex and thalamus are more deactivated than other regions of the brain (Franks, 2008). These regions are involved in the Global Neuronal Workspace theory of consciousness (Dehaene et al., 1998). In the awake condition, the non-human primate brain can detect unexpected deviations in auditory sequences as demonstrated by using the auditory “local-global” paradigm (Bekinschtein et al., 2009), with focal auditory activations for first-order violations (local violations) and activation of a large brain circuit including the prefrontal, parietal and cingulate cortices for second-order sequences (global violations) (Uhrig et al., 2014b) (Fig. 10). These results indicate that the ability to represent and predict the structure of auditory sequences is shared by humans (Bekinschtein et al., 2009) and NHPs (Uhrig et al., 2014b) and that the processing of high-order deviants activates in the macaque brain a fronto-parieto-cingular and thalamic network, similar and potentially homologous to the human Global Neuronal Workspace. The encoding of hierarchical auditory regularities is however, directly impacted by anesthesia and these neuronal consequences can differ depending on the anesthetic agent (Fig. 10) (Uhrig et al., 2016). Using fMRI, propofol, a GABA-ergic agonist, and ketamine, an NMDA antagonist administration, preserves the auditory cortical response to general auditory stimuli, probably by preserving the feedforward responses. These results show that some early sensory processing of external auditory stimuli is preserved during anesthesia and primary sensory cortices remain receptive to incoming sensory information during anesthesia. The local effect, reflecting the mismatch negativity (MMN) in electrophysiological studies, disappears during propofol anesthesia and shifts spatially during ketamine anesthesia compared to the awake state (Uhrig et al., 2016). In humans, the MMN is abolished during propofol-induced unconsciousness (Heinke et al., 2004). This “mismatch response” is thought to involve a violation of an expectation generated on the basis of initial tone repetition, which is thought to require a short-term plasticity of glutamatergic connections, either within the auditory cortex (Wacongne et al., 2012) or in long-distance projections from prefrontal cortex (Garrido et al., 2008). It should therefore not be surprising that this local effect disappears with anesthetics that affect these cortical circuits. Under increasing levels of propofol (ranging from moderate sedation to general anesthesia), a progressive disorganization of the global effect in the prefrontal, parietal and cingulate cortex is observed with a complete suppression under ketamine anesthesia. Thus, anesthetic agents disturb both short-term and long-term auditory predictive coding mechanisms in the macaque brain. This is a demonstration of how anesthetics can impact differently the task-evoked fMRI responses in NHPs. Finally, fMRI studies in macaques could show that, while stationary resting-state networks were preserved under general anesthesia (Vincent et al., 2007), the dynamical resting-state studies revealed a

massive reconfiguration of the repertoire of functional brain states under anesthesia (Barttfeld et al., 2015; Uhrig et al., 2018).

An alternative to the use of anesthesia as a means of ensuring compliance is to use physical restraint to prevent movement of the head during the imaging data acquisition. The best way to condition an animal to participate in imaging experiments while awake is to train and acclimate the animal to restraint using effective acclimatization protocols for NHPs. For example, in the procedures described in (Silva et al., 2011), marmosets can be trained for awake MRI in a few weeks, using a progressive acclimatization procedure that has benchmarks for evaluating the animal's progress and incorporating positive rewards for the completion of training sessions. The training starts with acclimating the animals to body restraint for increasingly long periods of time, followed by acclimatization of the animal to the typical sounds of the different MRI and fMRI pulse sequences, and finally introducing a rigid head restraint device in the last phase of the training (Silva et al., 2011). Each phase of the acclimatization procedure can be as short as a single week, but the actual duration should be adapted to each animal's response to the training, which can be quantified by a Behavioral Response Scale (Silva et al., 2011). For head fixation, several options have been shown to be effective, including the use of surgically implanted head-posts and chambers (Chen et al., 2017; Santisakultarm et al., 2016; Schaeffer et al., 2019) or non-invasive solutions such as the use of thermoplastic masks and helmets (Drucker et al., 2015; Srihasam et al., 2010) or customized 3D-printed helmets (Silva et al., 2011). Both methods have proven to be highly stable solutions, although the use of surgically implanted head-posts offers a more rigid restraint than the use of helmets (Hadj-Bouziane et al., 2014).

2. Using imaging methods for screening and monitoring health and pathology

Anatomical MRI scanning is of great benefit for NHP neuroscience research, both for the purposes of efficient experimental targeting as well as for long-term monitoring of the health and longevity of animals and implants (Balezeau et al., 2020). Such scanning is most effective when implants are non-metallic, and thus do not lead to large regions of dropout or distortion in the images, though the presence of relatively small amounts of titanium and other non-ferromagnetic materials often permit adequate scanning (i.e., they are safe but not necessarily compatible). Not only does the researcher need to consider potential artifacts created by metallic parts of the implant, we also need to keep in mind the induction of heat during scanning, which can lead to secondary injuries. In the previous sections, we discussed the use of anatomical MRI scanning, sometimes in coordination with X-ray CT scanning, to guide surgical planning, design MR-compatible chambers for 3D printing, and verify the intracranial positions of electrodes and other implants following the surgery. Here we focus on the health monitoring of experimental animals, and primarily the use of MRI to evaluate the integrity of cranial implants. We discuss early MRI-based signs of extracranial and intracranial infection and tissue growth, as well as the spectrum of interventions that can be applied before they become a major health risk. To the extent it is possible, routine anatomical health-check scans can greatly improve the health and welfare of chronically implanted animals, as well as success of the associated experiments. Although preventive

measures, such as routine, thorough cleaning of implants, and appropriate surgical placement and maintenance of implants, are vital to minimize the potential for infections, there is still a need for careful monitoring of the implant and surrounding tissues. Our focus is not on the preventative steps, but on the monitoring approaches, as this is an often-overlooked component in the long-term care of cranially implanted NHPs.

2.1. Early detection of tissue growth and infection under cranial implants

Over the course of approximately two decades, frequent scanning of cranially implanted NHPs has revealed a typical progression of events that can cause problems and, in some cases, lead to a brain infection. Prior to the availability of MRI scanning, the causes and progression of brain infections in NHP laboratories were often a matter of conjecture, sometimes bordering on superstition. However, careful inspection of the brain and head identified potential problems in apparently healthy animals, often long before clinical symptoms emerge. Most often, problems with chronic implants begin as seemingly innocuous granulation tissue growth at the margins of the implant. Such growth is common and has not been a general cause of concern for researchers. However, a quick MRI scan can in some cases, reveal that the tissue growth is not, in fact, confined to the margin but has begun to invade the space between the skull and the implant. This invasion can proceed along a portion of the implant edge, or is sometimes be confined to a single point, such as a physical opening between the implant and the bone, or the area around an insufficiently sealed screw.

On T1 MRI, tissue growth, primarily granulation tissue, or liquid can be identified as light gray or white (i.e. positive signal, or hyperintensity), which can stand out to the trained eye if sandwiched between the skull or implant materials, both of which generally appear as black (hypointensity). On T2 images the liquid and tissue growth would appear bright. Fig. 14 shows an example of fluid or tissue between the skull and an acrylic skull implant, where the thin stripe of light gray (yellow arrows) appears between the black underlying bone and the overlying acrylic layers. This pattern of granulation tissue growth is a common occurrence with skull implants composed of acrylic or dental cement, particularly if the curing process allows the implant edge to develop any irregularities, which trigger the normal granulation response. When left unchecked, such granulation tissue can overgrow underneath the implant and slowly lift the implant away from the skull; thus leading to the abrupt, and often unexpected, loss of the implant. The right half of Fig. 14 also shows an example of communication between the extracranial (green arrow) and intracranial (red arrow) space, in this case through a hole in the skull associated with a screw. In the NHP, most implants require several transcranial screws to fasten or anchor them to the skull, and degraded screw holes may provide a pathway for supracranial infections to enter into the epidural space. Careful application and curing of acrylic or dental cement, to generate a smooth texture and a solid monolithic implant that precisely meets the bone-skin interface, minimizes the formation of granulation tissue. This should be the goal of every approach to placement of any type of cranial implant, as minimizing granulation tissue formation will prolong the health of the implant, and of course, positively affect the health of the implanted NHP.

Each of the bright areas highlighted in Fig. 14 can be identified early and be treated as a potential problem that should be monitored closely. One common practice, for example, is to obtain a bacterial culture from suspicious areas to determine whether the MRI-visible incursion is associated with infection. Owing to the growing problem of antibiotic-resistant bacterial strains, it may not always be advisable to combat such warning signs with a general course of systemic antibiotics, though it is always good to make decisions with as much information as possible, in consultation with the attending veterinarians. Tracking potential sites of infection also allows for the planning of corrective measures, such as a surgical debridement to remove infected or exuberant tissue. Our extensive experience suggests that invasive or infected tissue, left unchecked over time, is apt to find its way into the intracranial space and pose a threat both to the animal's health and the course of the experiments.

In cases where MRI is unavailable or not appropriate (i.e., stainless steel implants), alternative imaging should be considered. While CT imaging alone is limited in its ability to detect infection in the soft tissues underneath the implant, use of single-photon emission computed tomography (SPECT) in conjunction with CT can provide precise anatomical mapping of infection (Fig. 15) (Guerriero et al., 2019).

There are several types of radiopharmaceuticals that can be used with SPECT; however, there is limited data on which type of radiopharmaceutical is most optimal for evaluating cranial implant infection in NHPs. ^{99m}Tc-hexamethylpropylene amine oxime (99mTc-HMPAO) is one such radiopharmaceutical that is commonly used for labeling neutrophils to localize inflammation and in fection in human medicine. The ^{99m}Tc-HMPAO complex can be taken up by all leukocytes but is selectively retained in neutrophils, due to chemical metabolism in the complex that prevents it from exiting the cell. This feature is useful for evaluating neutrophil-mediated processes of inflammation, such as bacterial infections that are commonly associated with cranial implants in NHPs. Because ^{99m}Tc has a short half-life of 6 hours, however, its ability to detect chronic indolent infections may be limited (Ballinger and Gnanasegaran, 2005). Rather, radiopharmaceuticals that have a longer half-life, such as ^{111}Indium (half-life, 67 h) may be more appropriate for slower developing infections (Love and Palestro, 2004; Roddie et al., 1988). Nonetheless, ^{99m}Tc-HMPAO has been shown to be more precise at differentiating soft tissue from bone infection, as compared with other radiopharmaceuticals (Filippi and Schillaci, 2006; Reuland et al., 1991).

In conjunction with a well-established routine of preventive care, the regular anatomical scanning of NHP subjects is of great value in the early detection and monitoring of infections, particularly for subjects with chronic implants, as well as for incidental issues that would affect research. The appearance of an infection often arises long after a surgical procedure and is often associated with an unwanted entry point at the margins of an implant. Some early signs of infection can be detected on MR images to those with a trained eye. Animals with chronic implants such as intracranial electrodes can sometimes acquire infections, commonly months or even years after a surgical procedure. In the absence of MRI scanning, such infections can go undetected and grow slowly until the animal displays clinical symptoms. If MRI is used to evaluate the brain only *after* animals exhibit clinical

symptoms, the images often reveal large and conspicuous signs of infection, such as an abscess of sufficient size to cause a midline displacement of the brain. When caught early, even deep brain infections are treated with success. For those extracranial infections that invade the space under the implant and those intracranial infections that have already become encapsulated, antibiotic treatment alone is less effective and surgical intervention is sometimes required. In all cases, clinical assessment and recovery is greatly aided by regular MRI scanning over subsequent weeks. The next section gives examples of several types of intracranial infections, as well as their response to treatment, in each case viewed through a series of anatomical MRI scans taken regularly after the infection was first detected.

2.2. Intracranial infections

An infection that enters the cranium through a hole in the skull, as discussed above, first occupies the epidural space, residing outside the dura mater, which can thicken to protect the brain for a period. If caught early, and with successful culturing of the infection, systemic antibiotics can usually reverse the progression of the infection, and in some cases clear it entirely. Fig. 16 shows an example of an infection both outside the skull, under the implant, and in the epidural space, detected and tracked using a series of T2-weighted MRI scans. The size of the epidural infection grew slightly during the first week of treatment and then began to shrink, such that it was largely gone after 7 weeks. While this type of decline is clearly a positive development that can temporarily hold an infection at bay, antibiotics alone are often ineffective at permanently removing an infection if it has a considerable presence under an implant. Thus, it is a good practice, once the infection is brought under control, to attempt a corrective surgical procedure to either physically flush the space or to remove the affected portion of the implant.

In the case that a transcranial infection is not detected at an early stage, an epidural abscess can form and enlarge to the point that it begins to displace brain tissue. An example of this situation is shown in Fig. 17, where an infection likely invaded the cranium through a screw hole under the implant and grew into an abscess. It bears emphasis that, in the absence of information gleaned from brain imaging, this process may proceed with only subtle or no clinical signs. Once an abscess becomes encapsulated, it is difficult to treat, because it consists essentially of a walled-off area of infection that lacks vascular penetration, and therefore systemic antibiotics are much less effective, or at best very slow in their action. Regarding the case depicted in Fig. 17 the initial approach was to begin a systemic antibiotic treatment in an attempt to combat the infection. In such a case, where there is no straightforward way to obtain a culture to test for bacterial type and resistance profiles, it is impossible to determine whether a given antibiotic will be effective. In this case, treatment proved entirely ineffective, as a scan ten days later showed that the abscess had grown significantly in size. In response to this information, an emergency surgery was performed, and the abscess was drained using a cannula and the cranial implant was entirely removed. During this procedure, the fluid from the abscess was submitted for analysis and the appropriate antibiotics were administered. This combination had the result of completely clearing the infection at all sites. Although the removal of the implant meant that the experimental work stopped, the animal recovered quickly, with only a small scar visible on

the MRI where the abscess had been previously and the animal ultimately returned to research successfully.

Thus, the routine MRI scan in this case alerted the investigators to the presence of the problem. The subsequent scan showed the growth of the problem and also provided critical information for a targeted surgical intervention, in this case a drainage of the abscess. Indeed, this approach is the standard of care in human neurology and neurosurgery, and should be emphasized in neuroscientific research as much as possible.

In the case of acute or chronic insertion of implants directly into the brain, such as microelectrodes or cannulae, infections can sometimes arise directly within deep brain tissue. Such cases can lead to encapsulated infections similar to that shown above, or to a broader encephalitis, and even ultimately to meningoencephalitis, any of which will greatly endanger the health of the animal and the viability of the experiments. One early warning sign for deep brain infections is the visualization of edema, usually as a bright patch on a T2-weighted scan, whose origin is often somewhere along the track of intracranial implants. Such edema can be invisible on typical T1-weighted anatomical scans, thus T2-scans are recommended for routine MRI health checks. In the example shown in Fig. 15, where there is a region of high signal intensity (hyperintensity, red arrow) diffusing from a portion of the implanted electrode, whose long vertical shadow is faintly visible. In this example, systemic antibiotics were administered the day of the detection, which led to a decrease in the observed edema six days later. In such cases, where deep infections have no clear communication to the extracranial space, systemic antibiotics can sometimes clear an infection entirely. In this particular case, there is a white stripe above the skull in the vicinity of the electrode penetration, thus the antibiotic treatment was only effective in the short term.

2.3. Incidental findings

Another area in which routine scanning is recommended is in the initial screening of NHPs destined for experiments. This practice can serve multiple purposes, including the acquisition of a high-quality anatomical scans for targeting, localization, implant design, or subsequent fMRI data as described above. One other use of this pre-experimental scan, however, is the screening for medical conditions or ano malies that might affect the research. One example of an incidental finding that occurred during a pre-surgical MRI scan assessment of an NHP selected for study appears in Fig. 19. This is hydrocephalus and is likely to be congenital resulting from cerebral aqueductal stenosis, as is seen in humans. Clearly, this individual would not be appropriate for neurologic research, unless that research was specific to this condition. The investigators used this scan to deselect the animal, who was known to have occasional mild to moderate seizures but was otherwise apparently healthy, even behaving appropriately, e.g., visually-guided movements.

3. Anesthesia protocols for clinical and experimental assessment using MRI

3.1. Pre-scan assessment: anesthesia

The use of MRI in neuroscientific research has revolutionized our ability to care for our research animals, especially NHP. Below we provide an overview of the anesthetic procedures we use to provide general clinical examination prior to MRI, as well as during MRI examination in both healthy and neurologically compromised NHP patients.

Blood collection is an important first step in assessment prior to MRI. Unless trained to present limbs for blood collection, even this routine clinical procedure requires anesthesia in NHP. Many facilities routinely use a ketamine, dexmedetomidine, and midazolam 'cocktail' for this procedure, as the sedative effects are easily and quickly reversible specifically with atipamezole and less specifically with yohimbine for the α^2 agonists, and flumazenil for the benzodiazepines. Based upon the need for the MRI - whether clinical or routine anatomic scans - blood testing may be skipped; however, any animal that has not had an assessment within six months should be considered a strong candidate for complete blood count (CBC), and a minimal blood chemistry, such as BUN, creatinine, electrolytes, liver enzymes, and total protein. Once the animal is anesthetized for blood collection, it is prudent to use that time to perform any other assessments, such as physical examination, ultrasonography, even radiographs, that may be deemed appropriate. The results of these tests will provide additional data for the clinical workup, and may help provide essential diagnostic evidence for treatments.

Next, an assessment of cardiovascular and respiratory function is recommended prior to administration of anesthesia for MRI. In the awake animal, cardiovascular and respiratory systems assessment include, respiratory rate and effort, whether normal, increased, or labored, any audible respiratory sounds such as wheezing, stertor, stridor, coughing, and color of visible mucosae to assess perfusion. Animals having difficulty breathing may also exhibit reluctance to move, panting without exertion or hyperthermia, and pale extremities. Physiological parameters should be monitored until the beginning of the anesthesia. Once sedated, auscultation, palpation, and EKG/ECG along with pulse oximetry provide a better picture of cardiopulmonary function. Although murmurs can be identified readily in otherwise normal animals, including humans, in NHPs murmurs should be documented for reassessment during future examinations. Once the animal is deemed stable or within normal limits, the animal can be transported to the MRI suite in accordance with facility policies. Depending on the reason for the scan, this preanesthetic assessment may be completed on the days before a scheduled MRI, or on the same day as the scan.

To prepare the animals for the anesthesia experiments, animals are fasted to prevent vomiting (six hours for solids and two hours for water). An antiemetic may also be provided. After the induction of anesthesia, the body temperature of the NHP can drop rapidly, because the animals can no longer regulate temperature and it is useful to put the NHP immediately on a heating blanket. Monkey eyes are protected with an ophthalmic lubricant (e.g., vitamin A cream) and the eyelids are gently closed to prevent eye dryness. For MRI

experiments, longer than one hour, intravenous hydration should be ensured by saline (0.9%) or a mixture of normal saline (0.9%) and glucose (5%) (250 ml of normal saline with 100 ml of 5% glucose) at a rate of 4–10 ml/kg/h i.v. (Uhrig et al., 2016).

3.2. Routine structural MRI scans: anesthesia

Anesthesia for routine structural MRI assessment can include a volatile anesthetic (1–3.0% ET isoflurane or 2–4% sevoflurane) or an intravenous bolus of ketamine, in combination as above (with careful attention to redosing schedules), or a different intravenous anesthetic such as propofol with constant rate infusion. A saline drip is often placed, to provide for hydration, and allows for immediate IV access should the animal develop critical needs. Routine monitoring of vital signs is critical. We recommend oxygen saturation and pulse rate with pulse oximetry (SpO_2) as well as capnography ($EtCO_2$), EKG, blood pressure, and respiratory rate. In general, maintaining the NHP patient in a light plane of anesthesia is preferred, primarily for scanning without movement artifacts. If movement becomes a concern, small doses of supplemental anesthesia or sedatives, such as dexmedetomidine or butorphanol, may be administered at this time. To avoid artifacts related to potential movements during MRI acquisition, a muscle blocking agent (for example, cisatracrium, 0.15 mg/kg bolus i.v. followed by continuous i.v. infusion at a rate of 0.18 mg/kg/h) could be used. It has to be noticed, that in this situation, the animal must be intubated and ventilated, as it is no longer breathing on its own. It is advisable that the muscle blocking agent be reversed before recovery from anesthesia. For anesthesia experiments, where monkeys were intubated and mechanically ventilated, they can be ventilated under a mixture of air/oxygen ($FiO_2 = 0.5$) with a tidal volume of 7–10 ml/kg aiming to normocapnic conditions. Before intubation, a local oropharyngal anesthesia (xylocaine) can be applied. Routine structural MRI do not normally require supplemental anesthesia, and any need for additional anesthetics should be done in consultation with the veterinarian.

3.3. Structural MRI assessment in compromised NHP: anesthesia

Unlike in human or veterinary clinical medicine, acute neurological illness in laboratory animal medicine usually results from a known source, either surgical complications, electrode trajectories, or experimental ablations. Unlike humans or other animals with traumatic brain injury or humans with stroke, laboratory NHPs are generally otherwise healthy and not showing multiple injuries with multiple organs involved, allowing us to focus primarily on the neurological disease. Even in humans with acute neurological lesions, anesthesia is a necessary part of the assessment and treatment paradigm. If the patient is obtunded or somnolent, they are managed with special attention to dose and anesthetic agent, intubated, mechanically ventilated and moved to surgery or imaging. Obtunded patients do not necessarily have any other issues, so monitoring their blood pressure, heart rate, SpO_2, $EtCO_2$, and managing those while the surgeon or MRI technician is performing their procedures, is the critical focus of the anesthetist. As is seen in humans, anesthesia allows the care staff to stabilize the blood pressure, which in turn benefits the CBF, and reduces the impact of the brain lesion.

The anesthetic agent used for a neurosurgical procedure ideally meets the following criteria: it does not increase intracranial pressure, is not epileptogenic, does not increase or even

decrease CBV, protects brain cells from ischemia, should not cause cardiovascular depression so that cerebral perfusion pressure is maintained and cerebral ischemia is prevented or pre-existing ischemia is not aggravated. The anesthesia should also be rapidly reversible so that the postoperative neurological status can be clinically assessed.

The effects of ketamine on cerebral physiology are controversial and conflicting. Some human and animal studies report that ketamine increases cerebral blood flow, cerebral metabolic rate, and intracranial pressure whereas others report no change or decreases in these parameters, particularly when ketamine is administered with other anesthetics (Chang et al., 2013). Given the uncertainty, we believe that ketamine should be used with caution for craniotomy, especially for patients with increased intracranial pressure. Ketamine is controversial, because its effects depend on patient variables, but some have held that it should not be used for animals that have pre-existing seizures because of the decoupling of excitation and inhibition. In our experience, even in animals with documented history of seizures, administration of ketamine does not routinely induce seizures, and we have successfully anesthetized animals with ketamine in seizure as well as those predisposed to seizures including animals with herniation and animals with serious cerebral edema. In animals that do have a history of seizures, regardless of the etiology, pre-medication with midazolam prior to anesthesia should be considered.

Each facility will have its own formulary, but published dosages range from 5–10 mg/kg IM of ketamine, combined with either diazepam, midazolam, dexmedetomidine, butorphanol, or other agents to provide muscle relaxation, sedation, and analgesia. Whether the anesthesia includes propofol is best discussed prior to any urgent request for anesthesia, as propofol requires intravenous administration, and can cause apnea, especially with deep sedation (general anesthesia). In this case, it seems preferable that the NHP be intubated and ventilated to avoid desaturation due to apnea. The use of propofol should always include the assessment for administration of analgesia by local, regional, or general anesthetics for analgesia, as propofol does not provide analgesia on its own. Researchers should develop the anesthetic protocols during the preliminary phases of their research projects, and not wait until they have emergencies.

A meta-analysis of intravenous anesthetic agents versus inhalant anesthetics found that while intracranial pressure tended to be higher in the inhalant group compared to the intravenous group, this did not result in any difference in surgical outcomes (Chui et al., 2014). This, along with the experience of the authors in performing anesthesia in NHP with neurological lesions, suggest that intracranial pressure can vary, even become elevated, without leading to adverse outcomes in the neurologically compromised patient. It is therefore recommended that veterinarians determine their anesthetic approach in the NHP without being overly cautious; using a balanced approach. Including injectable and inhalant anesthetics will provide a balanced, hemodynamically stable patient. It should be noticed, however, that volatile anesthetics, such as isoflurane and sevoflurane, induce cerebral vasodilation (Matta et al., 1999), especially at high dosage and isoflurane (with minimum alveolar concentration (MAC) > 1) increases the CBF Todd and Drummond (1984). Additional medications may be used judiciously, as determined by veterinary clinical assessment, for issues or other conditions not necessarily involving the brain.

A brief note to point out that while dexmedetomidine has been shown to cause reduced CBF due to its ability to induce vasoconstriction, it has variable effects upon neuroprotection depending on the species. In dogs, the decrease in cerebral blood flow is not accompanied by a decrease in cerebral metabolic rate, therefore placing the animals at risk of cerebral ischemia. In humans however, cerebral metabolic rate seems to be reduced along with cerebral blood flow. Studies are inconclusive thus far, and this requires further research. For up to date information see: https://www.uptodate.com/contents/anesthesia-for-craniotomy?sectionName=Anesthesia%20induction%20agents&topicRef=94283&anchor=H78577820&source=see_link#H78577820.

During neurosurgical procedures, it is advisable to maintain normocapnia during mechanical ventilation. The brief use of hypocapnia, in which ventilation parameters are modified to cause a drop in the $ETCO_2$ into a range between 28–30 mmHg, as a routine approach to control brain volume for functional imaging and for deep brain surgeries, while keeping in mind the possible influence of CO_2 on BOLD, is another area in which preparation and pre-planning will help mitigate post-procedural complications. It is necessary to keep in mind that prolonged hypocapnia leads to cerebral vasoconstriction, which can lead to cerebral ischemia, especially if there is an underlying brain lesion. When working with toxicity models, the induction of hypocapnia immediately, for any animal with suspected intracranial disease, and then adjust depending on what the localizer scans or the results of the early sequences show, gives the anesthetist a buffer zone for anesthetizing the neurological NHP. When working with models that involved neurotoxicity, either as a purpose of the research or as a complication, cerebral edema is very likely to occur. Hypocapnia has also been shown to be useful in anesthesia of patients with large intracranial abscesses.

If the researcher has the capability of performing imaging early (both baseline and early in the course of illness, post-operative conditions, and so on), as well as doing them frequently for all implanted animals, then hypocapnia is not required for every anesthetic period. An increase in brain volume is not always expected, and slow-growing space-occupying lesions are well-tolerated. The caveat here is whether the researcher has the ability to monitor CO_2 throughout the anesthetic period, or if they assume they can skip monitoring CO_2 because a diagnostic sequence is comparatively shorter than research sequences, but that is a risk that the investigator should discuss with the veterinarian, so that all parties are aware of the risk.

In our combined veterinary experience, anesthesia of the neurological patient involves the potential for complications, although careful attention to prevention will mitigate these. Adjusting doses for induction, combined with careful monitoring of vital parameters, and the potential brief use of hypocapnia, will enhance the survival of the neurological NHP. To avoid secondary brain damage, it is advisable to avoid hypovolemia, hypoxia, hypercapnia, hyperglycemia and pain during the neurosurgical procedure in the compromised NHP. Broadly speaking, the presence of central nervous system injury in research animals does not preclude anesthesia for MRI or other imaging modalities, and these modalities will allow for proper assessment of the patient, tracking the course of the illness - including the success or lack thereof in antibiotic or other treatment - and assist in the determination of prognosis. The veterinarian and principal investigator should prepare ahead of time, discussing possible outcomes and potential approaches, to minimize confusion when an emergent situation

arises. As always, prudent monitoring of all neurologically implanted animals provides for early intervention, thus reducing serious complications.

4. Combining behavioral and imaging assessment of well-being in non-human primates

To detect neurological problems, behavioral assessment is a powerful approach to complement regular MRI scans. Indeed, problems can occur between scheduled scans and daily behavioral checks can help determining when advancing the next MRI scan could be useful. A rigid posture, particularly with the head extended dorsally, head pressing, either against the cage or with the hands against the head; sensitivity to light (not photophobia, which is more severe); reluctance to move; lack of appetite; lack of interest in surroundings or lack of responsiveness other than to more intense stimuli can be signs of neurological problems. Change in normal behavior can also be used to recommend an earlier than normally scheduled scan. However, it requires determining what is normal behavior at baseline, not just for the species but also for the individual NHP. Most institutions with research programs involving NHP have some routine behavioral assessment plan in place, usually as checklists, to document the general demeanor, gross behavioral features including level of activity, alertness, and the presence or absence of stereotypies (Gauvin and Baird, 2008; Smith et al., 2006). The checklists facilitate detecting behavioral changes. When developing and performing behavioral assessments however, it is important to keep in mind a number of things. First, the presence of an observer may change the animals' behavior (Iredale et al., 2010). Although there is currently no evidence supporting the idea that NHPs mask their pain or other illness, the behavior an animal expresses upon observation has much to do with its familiarity with the observer and with being observed. Routine visits to the cage side with positive reinforcement, increases familiarity and thus decreases the likelihood of behavioral changes upon observation, thus leading to earlier and more accurate diagnoses (Raber et al., 2018). Collaborative working relationships between research and veterinary personnel are also critical, as research personnel generally have regular interactions with the animals and can detect subtle behavioral changes quickly. A way to minimize behavioral changes with observation is to use remote monitoring (Gaither et al., 2014). This approach can be successful, but careful consideration should be given to how or whether this information is stored, as it may be subject to public release upon request.

Besides neurological problems, routine husbandry and experimental procedures have the potential to induce chronic stress. Chronic stress can lead to poor psychological well-being and stress-related brain disorders. Many behaviors in NHPs are suspected to be indicators of chronic stress and poor psychological well-being (e.g. hair pulling, yawning, body shaking, self-grooming, self-scratching, self-injurious behaviors, diverse stereotypic behaviors, hunched posture). However, few have been fully validated. Consequently, when one assesses many behaviors, it is not uncommon for behaviors to vary in opposite directions (Gottlieb et al., 2013; Gray et al., 2016). Changes in behavior frequency are also usually too subtle to be detected via routine daily checks and might require behaviors to be systematically and precisely quantified. These examples highlight the need for rigorous testing and validation of

behavioral assessments to be used as measures of well-being in monkeys (Poirier and Bateson, 2017).

MRI can also be used to assess NHP psychological well-being, in addition to the monitoring of physiological health as described earlier. Indeed, a recent analysis suggests that measures of hippocampal volume or hippocampal local amount of gray matter allow tracking NHP well-being over months or years (Poirier et al., 2019). This MRI-based measures of welfare assessment presents many advantages: (1) they correlate with subjective psychological well-being and moods in humans; (2) they are sensitive to anti-depressant drugs in animal models, including NHPs; (3) they are sensitive to both deterioration and improvement of NHP well-being, changing in opposite directions depending of the valence of the experience (hippocampal plasticity increases with a positive experience and decreases with a negative one); (4) they are dose-dependent, the magnitude of the effect increasing with the duration or the number of positive or negative events an animal has been exposed to; (5) their sensitivity does not seem to be restricted to events that happened during early life, as they seem to detect exposure to positive and negative events during adulthood as well; (6) they are insensitive to short-lived variation in an individual well-being (plasticity changes within the hippocampus need to accumulate over several weeks to be detectable with MRI); and 7) they can be measured using a standard T1 weighted image (the sensitivity of the measure will nevertheless depend of the quality and resolution of the image), with some software providing the measure automatically (hippocampus volume only). However, a significant proportion of the inter-individual variability of hippocampal volume is inheritable (~ 40%). It is currently unknown whether this variation of genetic origin is linked to stress resilience and therefore to NHP well-being, or not. Based on current knowledge, this measure is thus not suitable for comparing well-being between individuals. We also do not know which absolute value of hippocampal volume/local amount of gray matter corresponds to a good status and which corresponds to a negative status. As a consequence, the interest of this measure relies on tracking changes in well-being within individuals over their lifetimes. It also offers the opportunity to measure scientifically the efficiency of any refinement attempt. For both applications, age effects need to be accounted for. Two measures are currently possible: the total volume of hippocampus and the local amount of gray matter in the anterior hippocampus. Although the second measure is suspected to be more sensitive to NHP well-being than the first, it remains to be further investigated.

5. Ethical considerations

A global legal requirement for neuroscientists using NHPs is to implement the 3Rs principle (Russell and Burch, 1959) of replacement, reduction and refinement (Mitchell et al., this issue). MRI offers many opportunities to refine experimental procedures routinely used in NHPs. Sharing a comprehensive picture of an animal's clinical health and well-being throughout a study, including the provision of adverse complications and subsequent remedies to improve animal welfare and minimize adverse complications, is critically important information that can impact the design and outcome of future research studies. Complications stemming from experimental procedures or otherwise, are not often described in papers (Olsson et al., 2008; Olsson et al., 2007). The lack of such reporting may result from concern that it could detract from the focus of the presented data or may be

misperceived by reviewers or by the public. However, failing to describe adverse complications as well as procedures to overcome obstacles, has potentially reduced opportunities for improvements in animal care and welfare.

Compared to electrophysiological experiments, which are typically performed in awake and alert NHPs, CT and MRI often usually, but not always as discussed above, require anesthesia. Both the neurological impact of multiple anesthetic events, and its possible impacts on psychological well-being of NHPs, require further investigation and needs to be considered. The potential welfare implications of repeated use of contrast agents and chelators sometimes used for specific applications of MRI also needs to be monitored (Prescott and Poirier, 2021).

6. Summary and conclusion

With the increase in the availability of imaging tools and procedures in research facilities, particularly MRI, we are now well-poised to make significant advances in improving the well-being, clinical care and experimental outcomes of laboratory NHPs. MRIs can be used to guide surgical planning and improve accuracy of brain structure targeting in NHPs, in much the same way that MRI is used to guide human neurosurgical procedures and treatments. MRI including fMRI, together with new software applications, can also be used to design and construct improved hardware for implantation which will extend the life expectancy of the implanted devices and enhance the overall care and well-being of the laboratory animals. When possible, routine MRIs can be performed to monitor animals' brain health over the course of their experimental lifetime, allowing for advanced screening of animals and potential rapid diagnosis and intervention, even before clinical signs appear. Attention to imaging modality as well as whether or not anesthesia is used and how, will further improve experimental and clinical outcomes. More recently, MRI of brain structures may even be used to assess well-being in laboratory NHPs allowing for the possible development of novel enrichment programs, validated using MRI, and designed to enhance psychological heath of laboratory NHPs. Our effort here is to provide information to scientists and veterinarians interested in taking advantage of modern imaging approaches at their facilities and to foster further discussions and interactions between scientists and veterinarians aimed at improving laboratory NHP well-being and health and experimental outcomes.

Funding sources

M.A.B. (R01EY13692, UF1NS107668, R01AG063090); S.K. (R01MH64043, R01EY017699, 21560-685 Silvio O. Conte Center); B.J. & L.U. (Foundation Bettencourt Schueller, France; Human Brain Project); D.A.L (ZIC MH002899); C.P. (Research fellowship from Newcastle University); A.C.S (R01NS117486, PA Dept. Health SAP 4100083102).

References

Adams DL, Economides JR, Jocson CM, Horton JC, 2007. A biocompatible titanium headpost for stabilizing behaving monkeys. J. Neurophysiol 98, 993–1001. [PubMed: 17522180]

Adams DL, Economides JR, Jocson CM, Parker JM, Horton JC, 2011. A water-tight acrylic-free titanium recording chamber for electrophysiology in behaving monkeys. J. Neurophysiol 106, 1581–1590. [PubMed: 21676928]

Aggleton JP, Passingham RE, 1981. Stereotaxic surgery under X-ray guidance in the rhesus monkey, with special reference to the amygdala. Exp. Brain Res 44, 271–276. [PubMed: 7030769]

Alkemade A, Schnitzler A, Forstmann BU, 2015. Topographic organization of the human and non-human primate subthalamic nucleus. Brain Struct. Funct 220, 3075–3086. [PubMed: 25921975]

Alvarez-Royo P, Clower RP, Zola-Morgan S, Squire LR, 1991. Stereotaxic lesions of the hippocampus in monkeys: determination of surgical coordinates and analysis of lesions using magnetic resonance imaging. J. Neurosci. Methods 38, 223–232. [PubMed: 1784125]

Amico E, Gomez F, Di Perri C, Vanhaudenhuyse A, Lesenfants D, Boveroux P, Bonhomme V, Brichant JF, Marinazzo D, Laureys S, 2014. Posterior cingulate cortex-related co-activation patterns: a resting state FMRI study in propofol-induced loss of consciousness. PLoS One 9, e100012. [PubMed: 24979748]

Amiez C, Sallet J, Hopkins WD, Meguerditchian A, Hadj-Bouziane F, Ben Hamed S, Wilson CRE, Procyk E, Petrides M, 2019. Sulcal organization in the medial frontal cortex provides insights into primate brain evolution. Nat. Commun 10, 3437. [PubMed: 31366944]

Andersen AH, Zhang Z, Barber T, Rayens WS, Zhang J, Grondin R, Hardy P, Gerhardt GA, Gash DM, 2002. Functional MRI studies in awake rhesus monkeys: methodological and analytical strategies. J. Neurosci. Methods 118, 141–152. [PubMed: 12204305]

Arcaro MJ, Honey CJ, Mruczek RE, Kastner S, Hasson U, 2015a. Widespread correlation patterns of fMRI signal across visual cortex reflect eccentricity organization. eLife 4.

Arcaro MJ, Pinsk MA, Kastner S, 2015b. The anatomical and functional organization of the human visual pulvinar. J. Neurosci 35, 9848–9871. [PubMed: 26156987]

Asahi T, Tamura R, Eifuku S, Hayashi N, Endo S, Nishijo H, Ono T, 2003. A method for accurate determination of stereotaxic coordinates in single-unit recording studies in monkeys by high-resolution three-dimensional magnetic resonance imaging. Neurosci. Res 47, 255–260. [PubMed: 14512151]

Assaf Y, Johansen-Berg H, Thiebaut de Schotten M, 2019. The role of diffusion MRI in neuroscience. NMR Biomed. 32, e3762. [PubMed: 28696013]

Balezeau et al., this issue

Ballinger JR, Gnanasegaran G, 2005. Radiolabelled leukocytes for imaging inflammation: how radiochemistry affects clinical use. Q. J. Nucl. Med. Mol. Imaging 49, 308–318.

Barttfeld P, Uhrig L, Sitt JD, Sigman M, Jarraya B, Dehaene S, 2015. Signature of consciousness in the dynamics of resting-state brain activity. Proc. Natl. Acad. Sci. USA 112, 887–892. [PubMed: 25561541]

Bekinschtein TA, Dehaene S, Rohaut B, Tadel F, Cohen L, Naccache L, 2009. Neural signature of the conscious processing of auditory regularities. Proc. Natl. Acad. Sci. USA 106, 1672–1677 [PubMed: 19164526]

Belcher AM, Yen CC, Notardonato L, Ross TJ, Volkow ND, Yang Y, Stein EA, Silva AC, Tomasi D, 2016. Functional connectivity hubs and networks in the awake marmoset brain. Front. Integr. Neurosci 10, 9. [PubMed: 26973476]

Bertrand H, Ellen YC, O'Keefe S, Flecknell PA, 2016. Comparison of the effects of ketamine and fentanyl-midazolam-medetomidine for sedation of rhesus macaques (Macaca mulatta). BMC Veterinary Res. 12 93–93.

Bertrand H, Sandersen C, Murray J, Flecknell PA, 2017. A combination of alfaxalone, medetomidine and midazolam for the chemical immobilization of Rhesus macaque (Macaca mulatta): preliminary results. J. Med. Primatol 46, 332–336. [PubMed: 28940590]

Biswal B, Yetkin FZ, Haughton VM, Hyde JS, 1995. Functional connectivity in the motor cortex of resting human brain using echo-planar MRI. Magn. Reson. Med 34, 537–541. [PubMed: 8524021]

Blonde JD, Roussy M, Luna R, Mahmoudian B, Gulli RA, Barker KC, Lau JC, Martinez-Trujillo JC, 2018. Customizable cap implants for neurophysiological experimentation. J. Neurosci. Methods 304, 103–117. [PubMed: 29694848]

Bola M, Barrett AB, Pigorini A, Nobili L, Seth AK, Marchewka A, 2018. Loss of consciousness is related to hyper-correlated gamma-band activity in anesthetized macaques and sleeping humans. NeuroImage 167, 130–142. [PubMed: 29162522]

Boveroux P, Vanhaudenhuyse A, Bruno MA, Noirhomme Q, Lauwick S, Luxen A, Degueldre C, Plenevaux A, Schnakers C, Phillips C, Brichant JF, Bonhomme V, Maquet P, Greicius MD, Laureys S, Boly M, 2010. Breakdown of within-and between-network resting state functional magnetic resonance imaging connectivity during propofol-induced loss of consciousness. Anesthesiology 113, 1038–1053. [PubMed: 20885292]

Buffalo EA, Movshon JA, Wurtz RH, 2019. From basic brain research to treating human brain disorders. Proc. Natl. Acad. Sci 116, 26167–26172.

Bukhari Q, Schroeter A, Cole DM, Rudin M, 2017. Resting state fMRI in mice reveals anesthesia specific signatures of brain functional networks and their interactions. Front Neural Circuits 11, 5. [PubMed: 28217085]

Bukhari Q, Schroeter A, Rudin M, 2018. Increasing isoflurane dose reduces homotopic correlation and functional segregation of brain networks in mice as revealed by resting-state fMRI. Sci. Rep 8, 10591. [PubMed: 30002419]

Chang LC, Raty SR, Ortiz J, Bailard NS, Mathew SJ, 2013. The emerging use of ketamine for anesthesia and sedation in traumatic brain injuries. Cns Neurosci. Ther 19, 390–395. [PubMed: 23480625]

Chen G, Wang F, Dillenburger BC, Friedman RM, Chen LM, Gore JC, Avi-son MJ, Roe AW, 2012. Functional magnetic resonance imaging of awake monkeys: some approaches for improving imaging quality. Magn. Reson. Imaging 30, 36–47. [PubMed: 22055855]

Chen X, Possel JK, Wacongne C, van Ham AF, Klink PC, Roelfsema PR, 2017. 3D printing and modelling of customized implants and surgical guides for non-human primates. J. Neurosci. Methods 286, 38–55. [PubMed: 28512008]

Chui J, Mariappan R, Mehta J, Manninen P, Venkatraghavan L, 2014. Comparison of propofol and volatile agents for maintenance of anesthesia during elective craniotomy procedures: systematic review and meta-analysis. Can. J. Anaesth 61, 347–356. [PubMed: 24482247]

Collier BD, Seltzer SE, Kido DK, Utsunomiya R, 1980. Ultrasound directed placement of needles into brains of rhesus monkeys. Neuroradiology 19, 201–205. [PubMed: 6770286]

Cox DD, Papanastassiou AM, Oreper D, Andken BB, Dicarlo JJ, 2008. High-resolution three-dimensional microelectrode brain mapping using stereo microfocal X-ray imaging. J. Neurophysiol 100, 2966–2976. [PubMed: 18815345]

Crawford K, Terasawa E, Kaufman PL, 1989. Reproducible stimulation of ciliary muscle contraction in the cynomolgus monkey via a permanent indwelling midbrain electrode. Brain Res. 503, 265–272. [PubMed: 2605519]

Dahl OE, Garvik LJ, Lyberg T, 1994. Toxic effects of methylmethacrylate monomer on leukocytes and endothelial cells in vitro. Acta. Orthop. Scand 65, 147–153. [PubMed: 8197846]

Daye PM, Monosov IE, Hikosaka O, Leopold DA, Optican LM, 2013. pyElectrode: an open-source tool using structural MRI for electrode positioning and neuron mapping. J. Neurosci. Methods 213, 123–131. [PubMed: 23261658]

Dehaene S, Kerszberg M, Changeux JP, 1998. A neuronal model of a global workspace in effortful cognitive tasks. Proc. Natl. Acad. Sci. USA 95, 14529–14534. [PubMed: 9826734]

Depprich R, Zipprich H, Ommerborn M, Naujoks C, Wiesmann HP, Kiattavorn-charoen S, Lauer HC, Meyer U, Kübler NR, Handschel J, 2008. Osseointegration of zirconia implants compared with titanium: an in vivo study. Head Face Med. 4, 30. [PubMed: 19077228]

Disbrow E, Roberts TPL, Slutsky D, Krubitzer L, 1999. The use of fMRI for determining the topographic organization of cortical fields in human and nonhuman primates. Brain Res. 829, 167–173. [PubMed: 10350543]

Dosenbach NU, Nardos B, Cohen AL, Fair DA, Power JD, Church JA, Nelson SM, Wig GS, Vogel AC, Lessov-Schlaggar CN, Barnes KA, Dubis JW, Feczko E, Coalson RS, Pruett JR Jr., Barch DM, Petersen SE, Schlaggar BL, 2010. Prediction of individual brain maturity using fMRI. Science 329, 1358–1361. [PubMed: 20829489]

Drucker CB, Carlson ML, Toda K, DeWind NK, Platt ML, 2015. Non-invasive primate head restraint using thermoplastic masks. J. Neurosci. Methods 253, 90–100. [PubMed: 26112334]

Drummond JC, 2019. Blood pressure and the brain: how low can you go? Anesth. Analg 128, 759–771. [PubMed: 30883421]

Dubowitz DJ, Chen DY, Atkinson DJ, Grieve KL, Gillikin B, Bradley WG Jr., Andersen RA, 1998. Functional magnetic resonance imaging in macaque cortex. Neuroreport 9, 2213–2218. [PubMed: 9694202]

Dubowitz DJ, Scadeng M, 2011. A frameless stereotaxic MRI technique for macaque neuroscience studies. Open Neuroimag J. 5, 198–205. [PubMed: 22253662]

Dunne NJ, Orr JF, 2002. Curing characteristics of acrylic bone cement. J. Mater. Sci. Mater. Med 13, 17–22. [PubMed: 15348199]

Duong TQ, 2010. Diffusion tensor and perfusion MRI of non-human primates. Methods 50, 125–135. [PubMed: 19665567]

Emborg ME, Joers V, Fisher R, Brunner K, Carter V, Ross C, Raghavan R, Brady M, Raschke J, Kubota K, Alexander A, 2010. Intraoperative intracerebral MRI-guided navigation for accurate targeting in nonhuman primates. Cell Transplant. 19, 1587–1597. [PubMed: 20587170]

Enchev Y, 2009. Neuronavigation: geneology, reality, and prospects. Neurosurg. Focus 27, E11.

Erhardt JB, Fuhrer E, Gruschke OG, Leupold J, Wapler MC, Hennig J, Stieglitz T, Korvink JG, 2018. Should patients with brain implants undergo MRI? J. Neural Eng 15, 041002. [PubMed: 29513262]

Fahlman A, Bosi EJ, Nyman G, 2006. Reversible anesthesia of Southeast Asian primates with medetomidine, zolazepam, and tiletamine. J. Zoo. Wildl Med 37, 558–561. [PubMed: 17315446]

Filippi L, Schillaci O, 2006. Usefulness of hybrid SPECT/CT in 99mTc-HMPAO-labeled leukocyte scintigraphy for bone and joint infections. J. Nucl. Med 47, 1908–1913. [PubMed: 17138732]

Fox MD, Zhang D, Snyder AZ, Raichle ME, 2009. The global signal and observed anticorrelated resting state brain networks. J Neurophysiol 101, 3270–3283. [PubMed: 19339462]

Franks NP, 2008. General anaesthesia: from molecular targets to neuronal pathways of sleep and arousal. Nat. Rev. Neurosci 9, 370–386. [PubMed: 18425091]

Frey S, Comeau R, Hynes B, Mackey S, Petrides M, 2004. Frameless stereotaxy in the nonhuman primate. NeuroImage 23, 1226–1234. [PubMed: 15528122]

Frey S, Pandya DN, Chakravarty MM, Bailey L, Petrides M, Collins DL, 2011. An MRI based average macaque monkey stereotaxic atlas and space (MNI monkey space). NeuroImage 55, 1435–1442. [PubMed: 21256229]

Fung SH, Burstein D, Born RT, 1998. In vivo microelectrode track reconstruction using magnetic resonance imaging. J. Neurosci. Methods 80, 215–224. [PubMed: 9667395]

Gaither AM, Baker KC, Gilbert MH, Blanchard JL, Liu DX, Luchins KR, Bohm RP, 2014. Videotaped behavior as a predictor of clinical outcome in rhesus macaques (Macaca mulatta). Comparative Med. 64, 193–199.

Gao Y, Mareyam A, Sun Y, Witzel T, Arango N, Kuang I, White J, Roe AW, Wald L, Stockmann J, Zhang X, 2020. A 16-channel AC/DC array coil for anesthetized monkey whole-brain imaging at 7T. NeuroImage 207, 116396. [PubMed: 31778818]

Garrido MI, Friston KJ, Kiebel SJ, Stephan KE, Baldeweg T, Kilner JM, 2008. The functional anatomy of the MMN: a DCM study of the roving paradigm. NeuroImage 42, 936–944. [PubMed: 18602841]

Gauthier CJ, Fan AP, 2019. BOLD signal physiology: Models and applications. NeuroImage 187, 116–127. [PubMed: 29544818]

Gauvin DV, Baird TJ, 2008. A functional observational battery in non-human primates for regulatory-required neurobehavioral assessments. J. Pharmacol. Toxicol. Methods 58, 88–93. [PubMed: 18586529]

Gearing M, Terasawa E, 1988. Luteinizing hormone releasing hormone (LHRH) neuroterminals mapped using the push-pull perfusion method in the rhesus monkey. Brain Res. Bull 21, 117–121. [PubMed: 3064879]

Ghahremani M, Hutchison RM, Menon RS, Everling S, 2017. Frontoparietal Functional Connectivity in the Common Marmoset. Cereb Cortex 27, 3890–3905. [PubMed: 27405331]

Glimcher PW, Ciaramitaro VM, Platt ML, Bayer HM, Brown MA, Handel A, 2001. Application of neurosonography to experimental physiology. J. Neurosci. Methods 108, 131–144. [PubMed: 11478972]

Goense JB, Logothetis NK, 2008. Neurophysiology of the BOLD fMRI signal in awake monkeys. Curr. Biol 18, 631–640. [PubMed: 18439825]

Goldman LW, 2007. Principles of CT and CT Technology. J. Nuclear Med. Technol 35, 115–128.

Golkowski D, Larroque SK, Vanhaudenhuyse A, Plenevaux A, Boly M, Di Perri C, Ranft A, Schneider G, Laureys S, Jordan D, Bonhomme V, Ilg R, 2019. Changes in whole brain dynamics and connectivity patterns during sevoflurane-and propofol-induced unconsciousness identified by functional magnetic resonance imaging. Anesthesiology 130, 898–911. [PubMed: 31045899]

Gómez F, Phillips C, Soddu A, Boly M, Boveroux P, Vanhaudenhuyse A, Bruno MA, Gosseries O, Bonhomme V, Laureys S, Noirhomme Q, 2013. Changes in effective connectivity by propofol sedation. PLoS One 8, e71370. [PubMed: 23977030]

Gottlieb DH, Coleman K, McCowan B, 2013. The effects of predictability in daily husbandry routines on captive rhesus macaques (Macaca mulatta). Appl. Animal Behav. Sci 143, 117–127.

Grandjean J, Schroeter A, Batata I, Rudin M, 2014. Optimization of anesthesia protocol for resting-state fMRI in mice based on differential effects of anesthetics on functional connectivity patterns. NeuroImage 102 (Pt 2), 838–847. [PubMed: 25175535]

Gray H, Bertrand H, Mindus C, Flecknell P, Rowe C, Thiele A, 2016. Physiological, behavioral, and scientific impact of different fluid control protocols in the rhesus macaque (Macaca mulatta). eNeuro 3 ENEURO.0195–0116.2016.

Grinvald A, Frostig RD, Siegel RM, Bartfeld E, 1991. High-resolution optical imaging of functional brain architecture in the awake monkey. Proc. Natl. Acad. Sci. USA 88, 11559–11563. [PubMed: 1763070]

Guerriero KA, Wilson SR, Sinusas AJ, Saperstein L, Zeiss AJ, 2019. Single-photon emission computed tomography-computed tomography using (99m)Tc-labeled leukocytes for evaluating infection associated with a cranial implant in a rhesus macaque (Macaca mulatta). Comp. Med 69, 249–256. [PubMed: 30935441]

Hadj-Bouziane F, Monfardini E, Guedj C, Gardechaux G, Hynaux C, Farnè A, Meunier M, 2014. The helmet head restraint system: a viable solution for resting state fMRI in awake monkeys. NeuroImage 86, 536–543. [PubMed: 24121168]

Heinke W, Kenntner R, Gunter TC, Sammler D, Olthoff D, Koelsch S, 2004. Sequential effects of increasing propofol sedation on frontal and temporal cortices as indexed by auditory event-related potentials. Anesthesiology 100, 617–625. [PubMed: 15108977]

Henderson JM, Tkach J, Phillips M, Baker K, Shellock FG, Rezai AR, 2005. Permanent neurological deficit related to magnetic resonance imaging in a patient with implanted deep brain stimulation electrodes for Parkinson's disease: case report. Neurosurgery 57, E1063 discussion E1063. [PubMed: 16284543]

Hess L, M •lek J, Kurzova A, Votava M, 2012. The effect of site (deltoid or glu-teus muscle) of intramuscular administration of anaesthetic drugs on the course of immobilisation in macaque monkeys (Macaca mulatta). Acta. Veterinaria Brno 81, 207–210.

Hori Y, Schaeffer DJ, Gilbert KM, Hayrynen LK, Cléry JC, Gati JS, Menon RS, Everling S, 2020a. Altered Resting-State Functional Connectivity Between Awake and Isoflurane Anesthetized Marmosets. Cereb Cortex.

Hori Y, Schaeffer DJ, Gilbert KM, Hayrynen LK, Cléry JC, Gati JS, Menon RS, Everling S, 2020b. Comparison of resting-state functional connectivity in marmosets with tracer-based cellular connectivity. NeuroImage 204, 116241. [PubMed: 31586676]

Horsely V, Clarke RH, 1908. The structure and functions of the cerebellum examined by a new method. Brain 31, 45–124.

Huang Z, Zhang J, Wu J, Liu X, Xu J, Zhang J, Qin P, Dai R, Yang Z, Mao Y, Hudetz AG, Northoff G, 2018. Disrupted neural variability during propofol-induced sedation and unconsciousness. Hum. Brain Mapp 39, 4533–4544. [PubMed: 29974570]

Hubel DH, Wiesel TN, 1962. Receptive fields, binocular interaction and functional architecture in the cat's visual cortex. J. Physiol 160, 106–154. [PubMed: 14449617]

Hudetz AG, 2012. General anesthesia and human brain connectivity. Brain Connect 2, 291–302. [PubMed: 23153273]

Hudetz AG, Liu X, Pillay S, 2015. Dynamic repertoire of intrinsic brain states is reduced in propofol-induced unconsciousness. Brain connectivity 5, 10–22. [PubMed: 24702200]

Hung CC, Yen CC, Ciuchta JL, Papoti D, Bock NA, Leopold DA, Silva AC, 2015. Functional MRI of visual responses in the awake, behaving marmoset. Neuroimage 120, 1–11. [PubMed: 26149609]

Hutchison RM, Gallivan JP, Culham JC, Gati JS, Menon RS, Everling S, 2012. Functional connectivity of the frontal eye fields in humans and macaque monkeys investigated with resting-state fMRI. J. Neurophysiol 107, 2463–2474. [PubMed: 22298826]

Hutchison RM, Hutchison M, Manning KY, Menon RS, Everling S, 2014. Isoflurane induces dose-dependent alterations in the cortical connectivity profiles and dynamic properties of the brain's functional architecture. Human Brain Mapp. 35, 5754–5775.

Hutchison RM, Womelsdorf T, Gati JS, Everling S, Menon RS, 2013. Resting-state networks show dynamic functional connectivity in awake humans and anesthetized macaques. Human Brain Mapp. 34, 2154–2177.

Hyder F, Rothman DL, Shulman RG, 2002. Total neuroenergetics support localized brain activity: implications for the interpretation of fMRI. Proc. Natl. Acad. Sci. USA 99, 10771–10776. [PubMed: 12134057]

Iredale SK, Nevill CH, Lutz CK, 2010. The influence of observer presence on baboon (Papio spp.) and rhesus macaque (Macaca mulatta) behavior. Appl. Animal Behav. Sci 122, 53–57.

Ishizawa Y, Ahmed OJ, Patel SR, Gale JT, Sierra-Mercado D, Brown EN, Eskandar EN, 2016. Dynamics of propofol-induced loss of consciousness across primate neocortex. J. Neurosci 36, 7718–7726. [PubMed: 27445148]

Janssen P, Verhoef BE, Premereur E, 2018. Functional interactions between the macaque dorsal and ventral visual pathways during three-dimensional object vision. Cortex 98, 218–227. [PubMed: 28258716]

Johnston JM, Cohen YE, Shirley H, Tsunada J, Bennur S, Christison-Lagay K, Veeder CL, 2016. Recent refinements to cranial implants for rhesus macaques (Macaca mulatta). Lab animal 45, 180–186. [PubMed: 27096188]

Jordan D, Ilg R, Riedl V, Schorer A, Grimberg S, Neufang S, Omerovic A, Berger S, Untergehrer G, Preibisch C, Schulz E, Schuster T, Schröter M, Spoormaker V, Zimmer C, Hemmer B, Wohlschläger A, Kochs EF, Schneider G, 2013. Simultaneous electroencephalographic and functional magnetic resonance imaging indicate impaired cortical top–down processing in association with anesthetic-induced unconsciousness. Anesthesiology 119, 1031–1042. [PubMed: 23969561]

Kalwani RM, Bloy L, Elliott MA, Gold JI, 2009. A method for localizing microelectrode trajectories in the macaque brain using MRI. J. Neurosci. Methods 176, 104–111. [PubMed: 18831988]

Kayser C, Petkov CI, Logothetis NK, 2009. Multisensory interactions in primate auditory cortex: fMRI and electrophysiology. Hear Res. 258, 80–88. [PubMed: 19269312]

Koyano KW, Machino A, Takeda M, Matsui T, Fujimichi R, Ohashi Y, Miyashita Y, 2011. In vivo visualization of single-unit recording sites using MRI-detectable elgiloy deposit marking. J. Neurophysiol 105, 1380–1392. [PubMed: 21123662]

Koyano Kenji W., Takeda M, Matsui T, Hirabayashi T, Ohashi Y, Miyashita Y, 2016. Laminar module cascade from layer 5 to 6 implementing cue-to-target conversion for object memory retrieval in the primate temporal cortex. Neuron 92, 518–529. [PubMed: 27720482]

Krzeminski D, Kaminski M, Marchewka A, Bola M, 2017. Breakdown of long-range temporal correlations in brain oscillations during general anesthesia. Neuroimage 159, 146–158. [PubMed: 28750775]

Krzemi ń ski D, Kami ń ski M, Marchewka A, Bola M, 2017. Breakdown of long-range temporal correlations in brain oscillations during general anesthesia. NeuroImage 159, 146–158. [PubMed: 28750775]

Kurtz SM, Devine JN, 2007. PEEK biomaterials in trauma, orthopedic, and spinal implants. Biomaterials 28, 4845–4869. [PubMed: 17686513]

Lee U, Ku S, Noh G, Baek S, Choi B, Mashour GA, 2013. Disruption of frontal–parietal communication by ketamine, propofol, and sevoflurane. Anesthesiology 118, 1264–1275. [PubMed: 23695090]

Lee VK, Flynt KS, Haag LM, Taylor DK, 2010. Comparison of the effects of ketamine, ketamine-medetomidine, and ketamine-midazolam on physiologic parameters and anesthesia-induced stress in rhesus (Macaca mulatta) and cynomolgus (Macaca fascicularis) macaques. J. Am. Assoc. Lab Anim. Sci 49, 57–63. [PubMed: 20122318]

Leopold DA, Murayama Y, Logothetis NK, 2003. Very slow activity fluctuations in monkey visual cortex: implications for functional brain imaging. Cereb Cortex 13, 422–433. [PubMed: 12631571]

Li CX, Patel S, Auerbach EJ, Zhang X, 2013. Dose-dependent effect of isoflurane on regional cerebral blood flow in anesthetized macaque monkeys. Neurosci. Lett 541, 58–62. [PubMed: 23428509]

Li CX, Patel S, Wang DJ, Zhang X, 2014. Effect of high dose isoflurane on cerebral blood flow in macaque monkeys. Magn. Reson Imaging 32, 956–960. [PubMed: 24890304]

Li CX, Zhang X, 2017. Effects of long-duration administration of 1% isoflurane on resting cerebral blood flow and default mode network in macaque monkeys. Brain Connect 7, 98–105. [PubMed: 28030956]

Li WX, Luo RY, Chen C, Li X, Ao JS, Liu Y, Yin YQ, 2019. Effects of propofol, dexmedetomidine, and midazolam on postoperative cognitive dysfunction in elderly patients: a randomized controlled preliminary trial. Chin. Med. J. (Engl) 132, 437–445. [PubMed: 30707179]

Liu JV, Hirano Y, Nascimento GC, Stefanovic B, Leopold DA, Silva AC, 2013. fMRI in the awake marmoset: somatosensory-evoked responses, functional connectivity, and comparison with propofol anesthesia. NeuroImage 78, 186–195. [PubMed: 23571417]

Liu X, Lauer KK, Douglas Ward B, Roberts C, Liu S, Gollapudy S, Rohloff R, Gross W, Chen G, Xu Z, Binder JR, Li S-J, Hudetz AG, 2017. Propofol attenuates low-frequency fluctuations of resting-state fMRI BOLD signal in the anterior frontal cortex upon loss of consciousness. NeuroImage 147, 295–301. [PubMed: 27993673]

Liu X, Yanagawa T, Leopold DA, Fujii N, Duyn JH, 2015a. Robust long-range coordination of spontaneous neural activity in waking. Sleep and Anesthesia. Cereb Cortex 25, 2929–2938. [PubMed: 24812083]

Liu X, Yanagawa T, Leopold DA, Fujii N, Duyn JH, 2015b. Robust long-range coordination of spontaneous neural activity in waking. Sleep and Anesthesia. Cerebral Cortex 25, 2929–2938. [PubMed: 24812083]

Logothetis NK, 2003a. MR imaging in the non-human primate: studies of function and of dynamic connectivity. Curr Opin Neurobiol 13, 630–642. [PubMed: 14630229]

Logothetis NK, 2003b. The underpinnings of the BOLD functional magnetic resonance imaging signal. J. Neurosci 23, 3963–3971. [PubMed: 12764080]

Logothetis NK, Guggenberger H, Peled S, Pauls J, 1999. Functional imaging of the monkey brain. Nat. Neurosci 2, 555–562. [PubMed: 10448221]

Love C, Palestro CJ, 2004. Radionuclide imaging of infection. J. Nucl. Med. Technol 32, 47–57 quiz 58–49. [PubMed: 15175400]

Lugo-Roman LA, Rico PJ, Sturdivant R, Burks R, Settle TL, 2010. Effects of serial anesthesia using ketamine or ketamine/medetomidine on hematology and serum biochemistry values in rhesus macaques (Macaca mulatta). J. Med. Primatol 39, 41–49. [PubMed: 19878432]

Lv P, Xiao Y, Liu B, Wang Y, Zhang X, Sun H, Li F, Yao L, Zhang W, Liu L, Gao X, Wu M, Tang Y, Chen Q, Gong Q, Lui S, 2016. Dose-dependent effects of isoflurane on regional activity and neural network function: a resting-state fMRI study of 14 rhesus monkeys: an observational study. Neurosci. Lett 611, 116–122. [PubMed: 26633103]

Maandag NJ, Coman D, Sanganahalli BG, Herman P, Smith AJ, Blumenfeld H, Shulman RG, Hyder F, 2007. Energetics of neuronal signaling and fMRI activity. Proc. Natl. Acad. Sci. USA 104, 20546–20551. [PubMed: 18079290]

Maciunas RJ, Galloway RL, 1989. Magnetic resonance and computed tomographic image-directed stereotaxy for animal research. Stereotact. Funct. Neurosurg 53, 197–201. [PubMed: 2701037]

Maier A, Wilke M, Aura C, Zhu C, Ye FQ, Leopold DA, 2008. Divergence of fMRI and neural signals in V1 during perceptual suppression in the awake monkey. Nat. Neurosci 11, 1193–1200. [PubMed: 18711393]

Mantini D, Hasson U, Betti V, Perrucci MG, Romani GL, Corbetta M, Orban GA, Vanduffel W, 2012a. Interspecies activity correlations reveal functional correspondence between monkey and human brain areas. Nat. Methods 9, 277–282. [PubMed: 22306809]

Mantini D, Hasson U, Betti V, Perrucci MG, Romani GL, Corbetta M, Orban GA, Vanduffel W, 2012b. Interspecies activity correlations reveal functional correspondence between monkey and human brain areas. Nat. Methods 9, 277–282. [PubMed: 22306809]

Masoud I, Shapiro F, Kent R, Moses A, 1986. A longitudinal study of the growth of the New Zealand white rabbit: cumulative and biweekly incremental growth rates for body length, body weight, femoral length, and tibial length. J. Orthop. Res 4, 221–231. [PubMed: 3712130]

Matsui T, Koyano KW, Koyama M, Nakahara K, Takeda M, Ohashi Y, Naya Y, Miyashita Y, 2007. MRI-based localization of electrophysiological recording sites within the cerebral cortex at single-voxel accuracy. Nat. Methods 4, 161–168. [PubMed: 17179936]

Matta BF, Heath KJ, Tipping K, Summors AC, 1999. Direct cerebral vasodilatory effects of sevoflurane and isoflurane. Anesthesiology 91, 677–680. [PubMed: 10485778]

McAndrew RM, Lingo VanGilder JL, Naufel SN, Helms Tillery SI, 2012. Individualized recording chambers for non-human primate neurophysiology. J. Neurosci. Methods 207, 86–90. [PubMed: 22498201]

Mitchell et al., this issue.

Mountcastle VB, 1997. The columnar organization of the neocortex. Brain 120 (Pt 4), 701–722. [PubMed: 9153131]

Mulliken GH, Bichot NP, Ghadooshahy A, Sharma J, Kornblith S, Philcock M, Desimone R, 2015. Custom-fit radiolucent cranial implants for neurophysiological recording and stimulation. J. Neurosci. Methods 241, 146–154. [PubMed: 25542350]

Nahm FKD, Dale AM, Albright TD, Amaral DG, 1994. In vivo microelectrode localization in the brain of the alert monkey: a combined radiographic and magnetic resonance imaging approach. Exp. Brain Res 98, 401–411. [PubMed: 8056063]

Nakahara K, Adachi Y, Osada T, Miyashita Y, 2007. Exploring the neural basis of cognition: multi-modal links between human fMRI and macaque neurophysiology. Trends Cogn. Sci 11, 84–92. [PubMed: 17188927]

Nelissen K, Vanduffel W, 2011. Grasping-related functional magnetic resonance imaging brain responses in the macaque monkey. J. Neurosci 31, 8220–8229. [PubMed: 21632943]

Ogawa S, Lee TM, Kay AR, Tank DW, 1990. In: Brain Magnetic Resonance Imaging with Contrast Dependent on Blood Oxygenation, 87. Proceedings of the National Academy of Sciences of the United States of America, pp. 9868–9872. [PubMed: 2124706]

Ohayon S, Tsao DY, 2012. MR-guided stereotactic navigation. J. Neurosci. Methods 204, 389–397. [PubMed: 22192950]

Olsson IA, Hansen AK, Sandøe P, 2008. Animal welfare and the refinement of neuroscience research methods–a case study of Huntington's disease models. Lab Anim. 42, 277–283. [PubMed: 18625582]

Olsson IAS, Hansen AK, Sandøe P, 2007. Ethics and refinement in animal research. Science 317 1680–1680.

Orban GA, 2016. Functional definitions of parietal areas in human and non-human primates. Proc. Biol. Sci 283.

Orban GA, Van Essen D, Vanduffel W, 2004. Comparative mapping of higher visual areas in monkeys and humans. Trends Cogn. Sci 8, 315–324. [PubMed: 15242691]

Ortiz-Rios M, Haag M, Balezeau F, Frey S, Thiele A, Murphy K, Schmid MC, 2018. Improved methods for MRI-compatible implants in nonhuman primates. J. Neurosci. Methods 308, 377–389. [PubMed: 30232039]

Overton JA, Cooke DF, Goldring AB, Lucero SA, Weatherford C, Recanzone GH, 2017. Improved methods for acrylic-free implants in nonhuman primates for neuroscience research. J. Neurophysiol 118, 3252–3270. [PubMed: 28855286]

Park S, Jang J, Kim J, Kim YS, Kim C, 2017. Real-time Triple-modal Photoacoustic, Ultrasound, and Magnetic Resonance Fusion Imaging of Humans. IEEE Trans. Med. Imaging 36, 1912–1921. [PubMed: 28436857]

Paxinos G, Huang XF, Toga AW, 2000. The Rhesus Monkey Brain in Stereotaxic Coordinates. Academic Press.

Paxinos G, Petrides M, Huang XF, Toga AW, 2008. The Rhesus Monkey Brain in Stereotaxic Coordinates. Elsevier Science.

Percheron G, Lacourly N, Albe-Fessard D, 1972. Lack of precision of thalamic stereotaxy based on cranial landmarks in some species of Macaca. Med. Primatol 2, 297–304.

Pezaris J, Dubowitz D, 1999. MRI Localization of Extracellular Electrodes using Metallic Deposition at 1.5T. Proc. Int. Soc. Magnetic Resonance Med 2.

Poirier C, Bateson M, 2017. Pacing stereotypies in laboratory rhesus macaques: Implications for animal welfare and the validity of neuroscientific findings. Neurosci. Biobehav. Rev 83, 508–515. [PubMed: 28893555]

Poirier C, Bateson M, Gualtieri F, Armstrong EA, Laws GC, Boswell T, Smulders TV, 2019. Validation of hippocampal biomarkers of cumulative affective experience. Neurosci. Biobehav. Rev 101, 113–121. [PubMed: 30951763]

Poirier et al., this issue

Pooley RA, 2005. Fundamental physics of MR imaging. Radiographics 25, 1087–1099. [PubMed: 16009826]

Poulen G, Chan Seng E, Menjot De Champfleur N, Cif L, Cyprien F, Perez J, Coubes P, 2020. Comparison between 1.5- and 3-T magnetic resonance acquisitions for direct targeting stereotactic procedures for deep brain stimulation: a phantom study. Stereotact Funct Neurosurg 1–8.

Power JD, Cohen AL, Nelson SM, Wig GS, Barnes KA, Church JA, Vogel AC, Laumann TO, Miezin FM, Schlaggar BL, Petersen SE, 2011. Functional network organization of the human brain. Neuron 72, 665–678. [PubMed: 22099467]

Premereur E, Decramer T, Coudyzer W, Theys T, Janssen P, 2020. Localization of movable electrodes in a multi-electrode microdrive in nonhuman primates. J. Neurosci. Methods 330, 108505. [PubMed: 31711885]

Prescott MJ, Poirier C, 2021. The role of MRI in applying the 3Rs to non-human primate neuroscience. NeuroImage 225, 117521. [PubMed: 33137476]

Pró-Sistiaga P, Lamberton F, Boraud T, Saulnier R, Young AR, Bioulac B, Gross C, Mazoyer B, 2012. High resolution 3T fMRI in anesthetized monkeys. J. Neurosci. Methods 205, 86–95. [PubMed: 22230769]

Pulley AC, Roberts JA, Lerche NW, 2004. Four preanesthetic oral sedation protocols for rhesus macaques (Macaca mulatta). J. Zoo Wildl Med 35, 497–502. [PubMed: 15732590]

Raabe A, Krishnan R, Wolff R, Hermann E, Zimmermann M, Seifert V, 2002. Laser surface scanning for patient registration in intracranial image-guided surgery. Neurosurgery 50, 797–803. [PubMed: 11904031]

Raber JM, Niekrasz M, Linkenhoker J, Perdue KA, 2018. Veterinary Care. In: We-ichbrod RH, Thompson GA, Norton JN (Eds.), Management of Animal Care and Use Programs in Research, Education, and Testing. CRC Press/Taylor & Francis, Boca Raton (FL).

Ranft A, Golkowski D, Kiel T, Riedl V, Kohl P, Rohrer G, Pientka J, Berger S, Thul A, Maurer M, Preibisch C, Zimmer C, Mashour GA, Kochs EF, Jordan D, Ilg R, 2016. Neural correlates of sevoflurane-induced unconsciousness identified by simultaneous functional magnetic resonance imaging and electroencephalography. Anesthesiology 125, 861–872. [PubMed: 27617689]

Rebert CS, Hurd RE, Matteucci MJ, De LaPaz R, Enzmann DR, 1991. A procedure for using proton magnetic resonance imaging to determine stereotaxic coordinates of the monkey's brain. J. Neurosci. Methods 39, 109–113. [PubMed: 1798341]

Reuland P, Winker KH, Heuchert T, Ruck P, Müller-Schauenburg W, Weller S, Feine U, 1991. Detection of infection in postoperative orthopedic patients with technetium-99m-labeled monoclonal antibodies against granulocytes. J. Nucl. Med 32, 2209–2214. [PubMed: 1744705]

Reveley C, Gruslys A, Ye FQ, Glen D, Samaha J, B ER, Saad Z, A KS, Leopold DA, Saleem KS, 2017. Three-dimensional digital template atlas of the macaque brain. Cereb Cortex 27, 4463–4477. [PubMed: 27566980]

Roddie ME, Peters AM, Danpure HJ, Osman S, Henderson BL, Lavender JP, Carroll MJ, Neirinckx RD, Kelly JD, 1988. Inflammation: imaging with Tc-99m HMPAO-labeled leukocytes. Radiology 166, 767–772. [PubMed: 3340775]

Russell WMS, Burch RL, 1959. The Principles of Humane Experimental Technique. Methuen & Co., London.

Russell WMS, Burch RL, 1959. The Principles of Humane Experimental Technique. Methuen, London ISBN 0900767782.

Saalmann YB, Pinsk MA, Wang L, Li X, Kastner S, 2012. The pulvinar regulates information transmission between cortical areas based on attention demands. Science 337, 753–756. [PubMed: 22879517]

Saleem K, Logothetis N, 2007. A combined MRI and Histology Atlas of the Rhesus Monkey Brain in Stereotaxic Coordinates. Elsevier, London.

Santisakultarm TP, Kersbergen CJ, Bandy DK, Ide DC, Choi SH, Silva AC, 2016. Two-photon imaging of cerebral hemodynamics and neural activity in awake and anesthetized marmosets. J. Neurosci. Methods 271, 55–64. [PubMed: 27393311]

Saunders RC, Aigner TG, Frank JA, 1990. Magnetic resonance imaging of the rhesus monkey brain: use for stereotactic neurosurgery. Exp. Brain Res 81, 443–446. [PubMed: 2204546]

Schaeffer DJ, Gilbert KM, Hori Y, Gati JS, Menon RS, Everling S, 2019. Integrated radiofrequency array and animal holder design for minimizing head motion during awake marmoset functional magnetic resonance imaging. Neuroimage 193, 126–138. [PubMed: 30879997]

Schlaier J, Warant J, Brawanski A, 2002. Registration accuracy and practicability of laser-directed surface matching. Cmput. Aided Surg 7, 284–290.

Seidlitz J, Sponheim C, Glen D, Ye FQ, Saleem KS, Leopold DA, Ungerleider L, Messinger A, 2018. A population MRI brain template and analysis tools for the macaque. NeuroImage 170, 121–131. [PubMed: 28461058]

Settle TL, Rico PJ, Lugo-Roman LA, 2010. The effect of daily repeated sedation using ketamine or ketamine combined with medetomidine on physiology and anesthetic characteristics in rhesus macaques. J. Med. Primatol 39, 50–57. [PubMed: 19912466]

Shamir RR, Freiman M, Joskowicz L, Spektor S, Shoshan Y, 2009. Surface-based facial scan registration in neuronavigation procedures: a clinical study. J. Neurosurg 111, 1201–1206. [PubMed: 19392604]

Sharma S, Mantini D, Vanduffel W, Nelissen K, 2019. Functional specialization of macaque premotor F5 subfields with respect to hand and mouth movements: A comparison of task and resting-state fMRI. Neuroimage 191, 441–456. [PubMed: 30802514]

Sheffield JM, Barch DM, 2016. Cognition and resting-state functional connectivity in schizophrenia. Neurosci. Biobehav. Rev 61, 108–120. [PubMed: 26698018]

Sicard KM, Duong TQ, 2005. Effects of hypoxia, hyperoxia, and hypercapnia on baseline and stimulus-evoked BOLD, CBF, and CMRO2 in spontaneously breathing animals. NeuroImage 25, 850–858. [PubMed: 15808985]

Silva AC, 2017. Anatomical and functional neuroimaging in awake, behaving marmosets. Develop. Neurobiol 77, 373–389.

Silva AC, Liu JV, Hirano Y, Leoni RF, Merkle H, Mackel JB, Zhang XF, Nascimento GC, Stefanovic B, 2011. Longitudinal functional magnetic resonance imaging in animal models. Methods Mol. Biol 711, 281–302. [PubMed: 21279608]

Smith JJ, Hadzic V, Li X, Liu P, Day T, Utter A, Kim B, Washington IM, Basso MA, 2006. Objective measures of health and well-being in laboratory rhesus monkeys (Macaca mulatta). J. Med. Primatol 35, 388–396. [PubMed: 17214668]

Snider RS, Lee JC, 1961. A Stereotaxic Atlas of the Monkey Brain. University of Chicago Press.

Sporns O, Honey CJ, 2013. Topographic dynamics in the resting brain. Neuron 78, 955–956. [PubMed: 23791191]

Srihasam K, Sullivan K, Savage T, Livingstone MS, 2010. Noninvasive functional MRI in alert monkeys. Neuroimage 51, 267–273. [PubMed: 20116433]

Standage D, Areshenkoff CN, Nashed JY, Hutchison RM, Hutchison M, Heinke D, Menon RS, Everling S, Gallivan JP, 2020. Dynamic reconfiguration, fragmentation, and integration of whole-brain modular structure across depths of unconsciousness. Cerebral Cortex.

Stefanacci L, Reber P, Costanza J, Wong E, Buxton R, Zola S, Squire L, Albright T, 1998. fMRI of monkey visual cortex. Neuron 20, 1051–1057. [PubMed: 9655492]

Stübinger S, Drechsler A, Bürki A, Klein K, Kronen P, von Rechenberg B, 2016. Titanium and hydroxyapatite coating of polyetheretherketone and carbon fiber-rein-forced polyetheretherketone: a pilot study in sheep. J. Biomed.Mater. Res. Part B 104, 1182–1191.

Sun FJ, Wright DE, Pinson DM, 2003. Comparison of ketamine versus combination of ketamine and medetomidine in injectable anesthetic protocols: chemical immobilization in macaques and tissue reaction in rats. Contemp Top Lab Anim. Sci 42, 32–37. [PubMed: 12906399]

Szabo J, Cowan WM, 1984. A stereotaxic atlas of the brain of the cynomolgus monkey (Macaca fascicularis). J. Comparative Neurol 222, 265–300.

Talbot T, Ide D, Liu N, Turchi J, 2012. A novel, variable angle guide grid for neuronal activity studies. Front. Integr. Neurosci 6.

Tammer R, Ehrenreich L, Boretius S, Watanabe T, Frahm J, Michaelis T, 2006. Compatibility of glass-guided recording microelectrodes in the brain stem of squirrel monkeys with high-resolution 3D MRI. J. Neurosci. Methods 153, 221–229. [PubMed: 16343640]

Tani N, Joly O, Iwamuro H, Uhrig L, Wiggins CJ, Poupon C, Kolster H, Vanduffel W, Le Bihan D, Palfi S, Jarraya B, 2011. Direct visualization of non-human primate subcortical nuclei with contrast-enhanced high field MRI. NeuroImage 58, 60–68. [PubMed: 21704174]

Todd MM, Drummond JC, 1984. A comparison of the cerebrovascular and metabolic effects of halothane and isoflurane in the cat. Anesthesiology 60, 276–282. [PubMed: 6703382]

Tokuno H, Hatanaka N, Takada M, Nambu A, 2000. B-mode and color Doppler ultrasound imaging for localization of microelectrode in monkey brain. Neurosci. Res 36, 335–338. [PubMed: 10771112]

Tootell RB, Tsao D, Vanduffel W, 2003. Neuroimaging weighs in: humans meet macaques in “primate” visual cortex. J Neurosci 23, 3981–3989. [PubMed: 12764082]

Tsao D, 2014. The macaque face patch system: a window into object representation. Cold Spring Harb Symp Quant Biol 79, 109–114. [PubMed: 25943770]

Tsao DY, Livingstone MS, 2008. Mechanisms of face perception. Ann. Rev. Neurosci 31, 411–437. [PubMed: 18558862]

Tsukada H, Sato K, Kakiuchi T, Nishiyama S, 2000. Age-related impairment of coupling mechanism between neuronal activation and functional cerebral blood flow response was restored by cholinesterase inhibition: PET study with microdialysis in the awake monkey brain. Brain Res. 857, 158–164. [PubMed: 10700563]

Uhrig L, Ciobanu L, Djemai B, Le Bihan D, Jarraya B, 2014a. Sedation agents differentially modulate cortical and subcortical blood oxygenation: evidence from ultra-high field MRI at 17.2 T. PLoS One 9, e100323. [PubMed: 25050866]

Uhrig L, Dehaene S, Jarraya B, 2014b. A hierarchy of responses to auditory regularities in the macaque brain. J. Neurosci 34, 1127–1132. [PubMed: 24453305]

Uhrig L, Janssen D, Dehaene S, Jarraya B, 2016. Cerebral responses to local and global auditory novelty under general anesthesia. NeuroImage 141, 326–340. [PubMed: 27502046]

Uhrig L, Sitt JD, Jacob A, Tasserie J, Barttfeld P, Dupont M, Dehaene S, Jarraya B, 2018. Resting-state dynamics as a cortical signature of anesthesia in monkeys. Anesthesiology 129, 942–958. [PubMed: 30028727]

Vanduffel W, Fize D, Mandeville JB, Nelissen K, Van Hecke P, Rosen BR, Tootell RB, Orban GA, 2001. Visual motion processing investigated using contrast agent-enhanced fMRI in awake behaving monkeys. Neuron 32, 565–577. [PubMed: 11719199]

Vincent JL, Patel GH, Fox MD, Snyder AZ, Baker JT, Van Essen DC, Zempel JM, Snyder LH, Corbetta M, Raichle ME, 2007. Intrinsic functional architecture in the anaesthetized monkey brain. Nature 447, 83–86. [PubMed: 17476267]

Wacongne C, Changeux J-P, Dehaene S, 2012. A neuronal model of predictive coding accounting for the mismatch negativity. J. Neurosci 32, 3665–3678. [PubMed: 22423089]

Wagman I, Loeffler J, McMillan J, 1975. Relationship between growth of brain and skull of macaca mulatta, and its importance for the stereotaxic technique. Brain, Behav. Evol 12, 116–134. [PubMed: 811323]

Walbridge S, Murad GJA, Heiss JD, Oldfield EH, Lonser RR, 2006. Technique for enhanced accuracy and reliability in non-human primate stereotaxy. J. Neurosci. Methods 156, 310–313. [PubMed: 16516975]

Wang L, Saalmann YB, Pinsk MA, Arcaro MJ, Kastner S, 2012. Electrophysiological low-frequency coherence and cross-frequency coupling contribute to BOLD connectivity. Neuron 76, 1010–1020. [PubMed: 23217748]

Wang R, Foniok T, Wamsteeker JI, Qiao M, Tomanek B, Vivanco RA, Tuor UI, 2006. Transient blood pressure changes affect the functional magnetic resonance imaging detection of cerebral activation. NeuroImage 31, 1–11. [PubMed: 16460967]

Wang Z, Chen LM, Négyessy L, Friedman RM, Mishra A, Gore JC, Roe AW, 2013. The relationship of anatomical and functional connectivity to resting-state connectivity in primate somatosensory cortex. Neuron 78, 1116–1126. [PubMed: 23791200]

Willems P, Berkelbach van der Sprenkel J, Tulleken C, 2001. Comparison of Adhesive Markers, Anatomical Landmarks, and Surface Matching in Patient-To-Image Registration for Frameless Stereotaxy. SPIE.

Wilson GH 3rd, Yang PF, Gore JC, Chen LM, 2016. Correlated inter-regional variations in low frequency local field potentials and resting state BOLD signals within S1 cortex of monkeys. Hum. Brain Mapp 37, 2755–2766. [PubMed: 27091582]

Wu T-L, Mishra A, Wang F, Yang P-F, Gore JC, Chen LM, 2016. Effects of isoflurane anesthesia on resting-state fMRI signals and functional connectivity within primary somatosensory cortex of monkeys. Brain Behav 6 e00591–e00591. [PubMed: 28032008]

Wu X, Yang Z, Bailey SK, Zhou J, Cutting LE, Gore JC, Ding Z, 2017. Functional connectivity and activity of white matter in somatosensory pathways under tactile stimulations. NeuroImage 152, 371–380. [PubMed: 28284801]

Yamada Y, Matsumoto Y, Okahara N, Mikoshiba K, 2016. Chronic multiscale imaging of neuronal activity in the awake common marmoset. Sci. Rep 6, 35722. [PubMed: 27786241]

Young SS, Schilling AM, Skeans S, Ritacco G, 1999. Short duration anaesthesia with medetomidine and ketamine in cynomolgus monkeys. Lab Anim. 33, 162–168. [PubMed: 10780820]

Zhang Z, Cai D-C, Wang Z, Zeljic K, Wang Z, Wang Y, 2019. Isoflurane-induced burst suppression increases intrinsic functional connectivity of the monkey brain. Front. Neurosci 13 296–296. [PubMed: 31031580]

Fig. 1.

Example axial (horizontal) CT image from a human showing the hyperdense signal arising from the bony skull and an intraparenchymal hemorrhage.

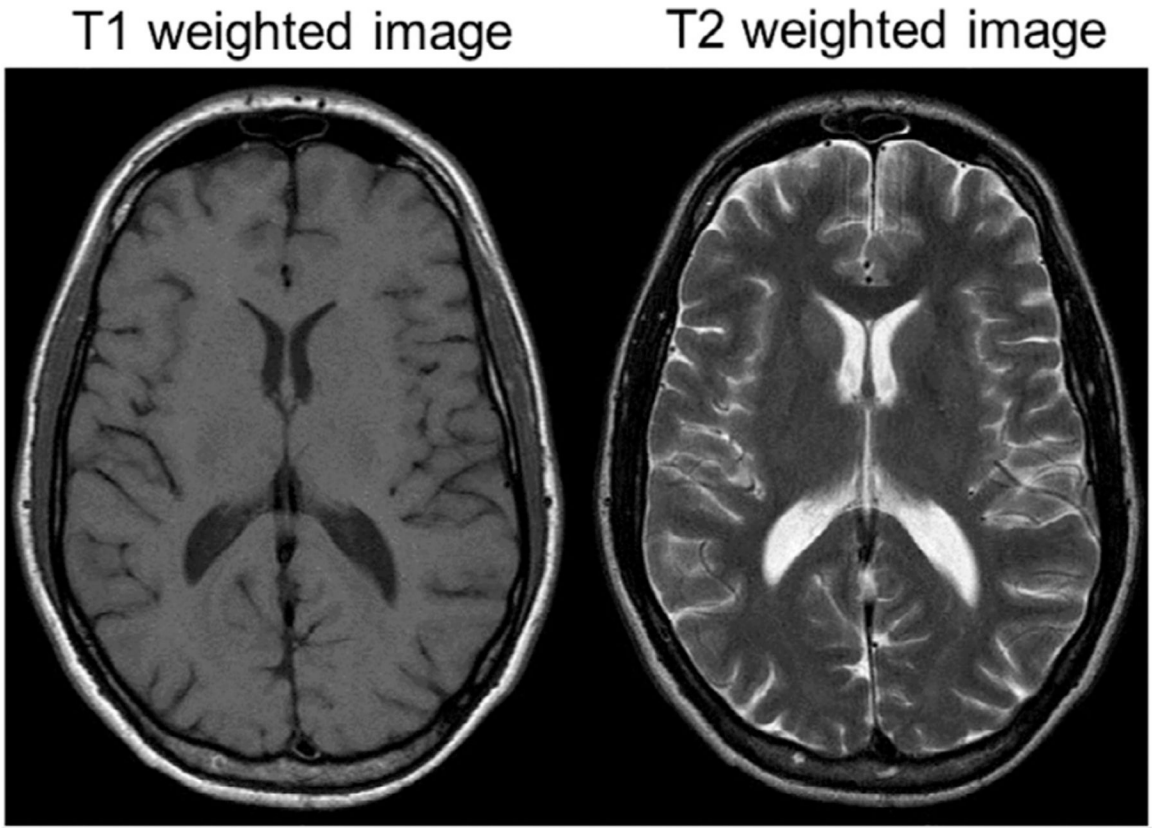

Fig. 2.

Example horizontal sections showing a T1 (left) and T2 (right) weighted images from a human brain. Note CSF hyperintensity in the T2 image and hypointensity in the T1 weighted image.

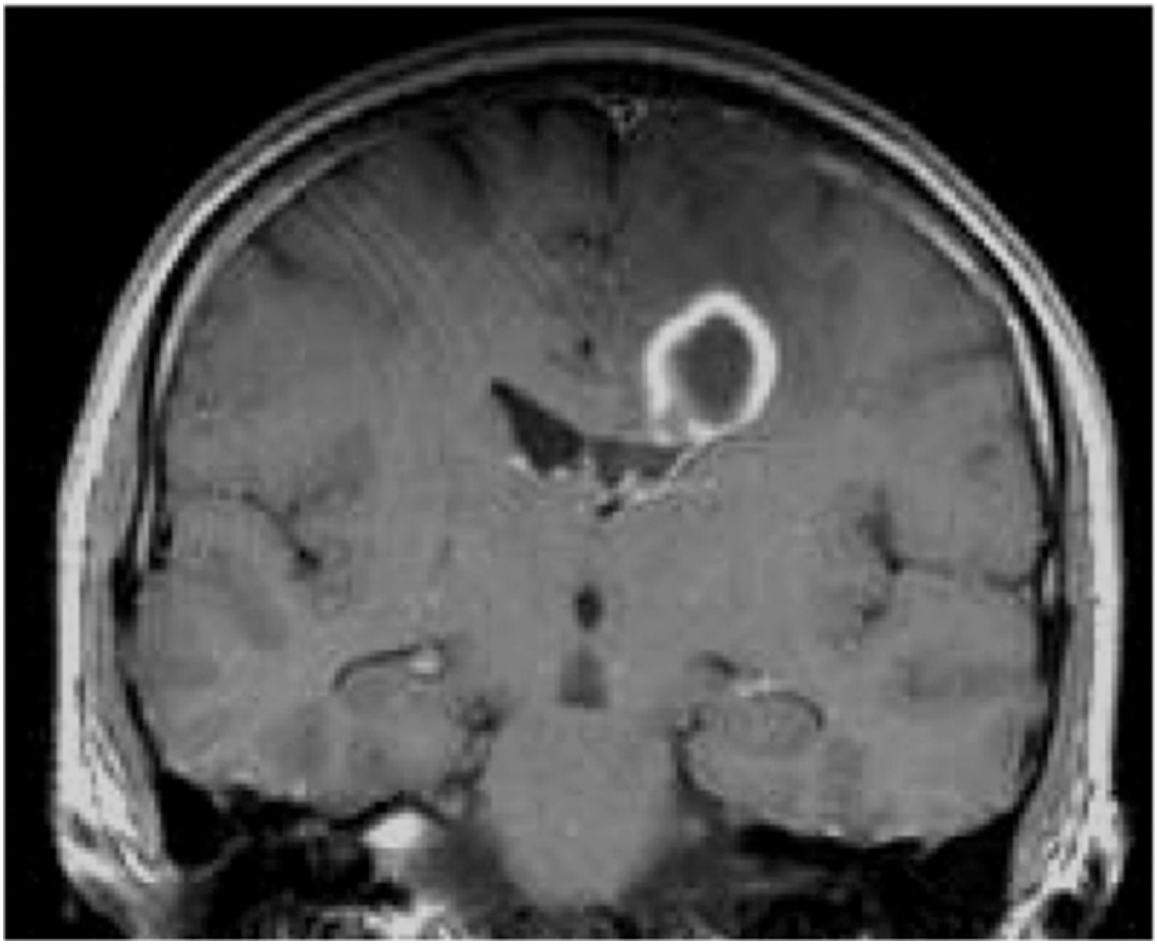

Fig. 3.
Coronal T1 weighted post contrast image of an intraparenchymal abscess in a human brain.

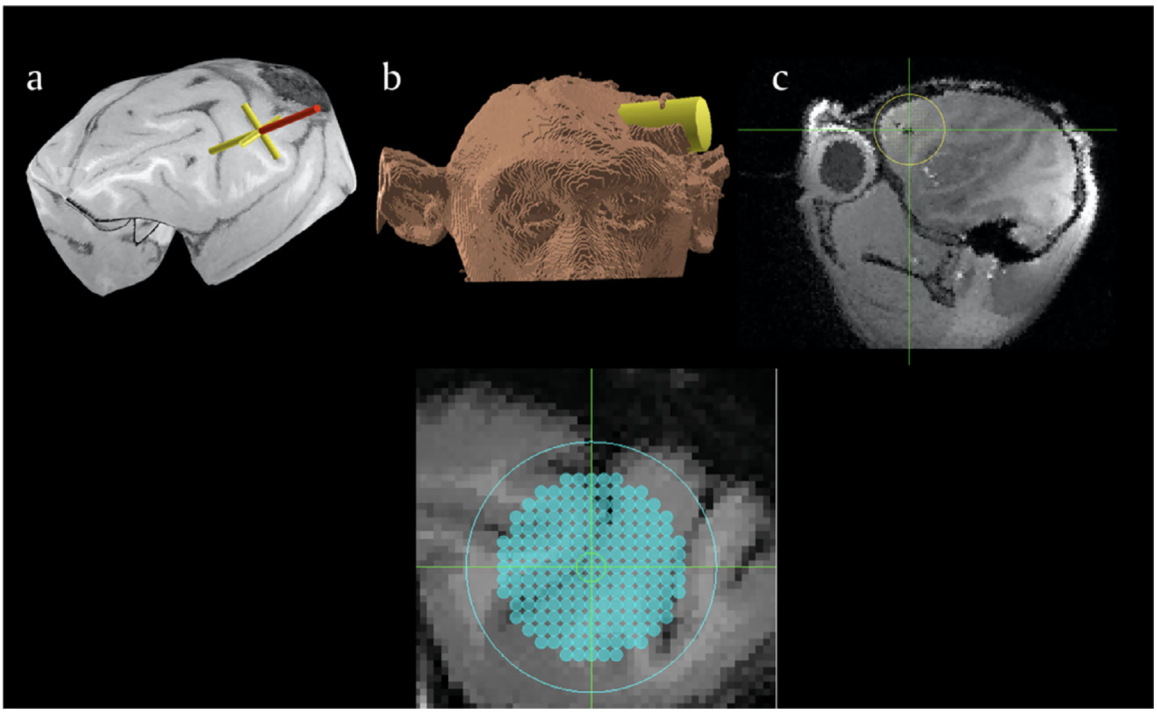

Fig. 4.

a. Planning software allows researchers to identify a region of interest on the MRI and reconstructed surfaces of the brain; b. simulation of an electrophysiology chamber over the planned target location at the appropriate angle; c) visualization of the x-y electrode placements. The lower image shows a grid positioned and superimposed on the brain MRI. Adapted from Frey et al., 2007.

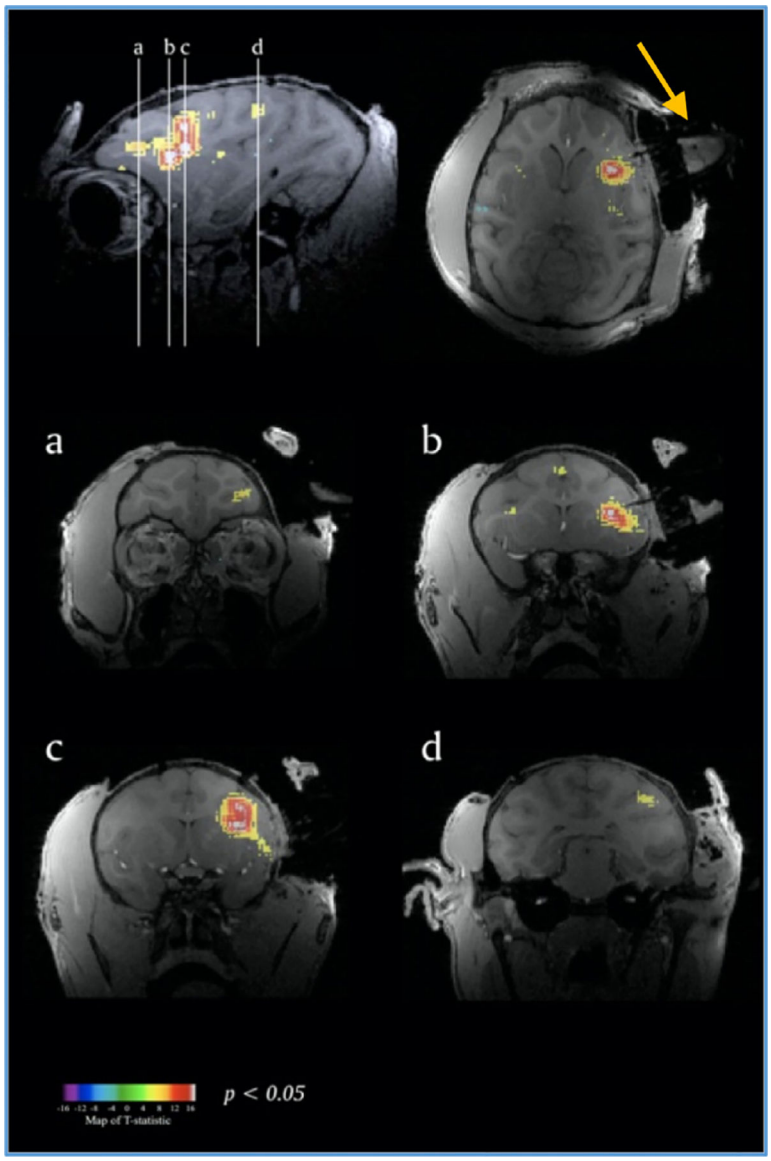

Fig. 5.

Functional imaging data in frontal lobe of the NHP used to help place recording chamber (arrow). Adapted from Frey et al., 2007

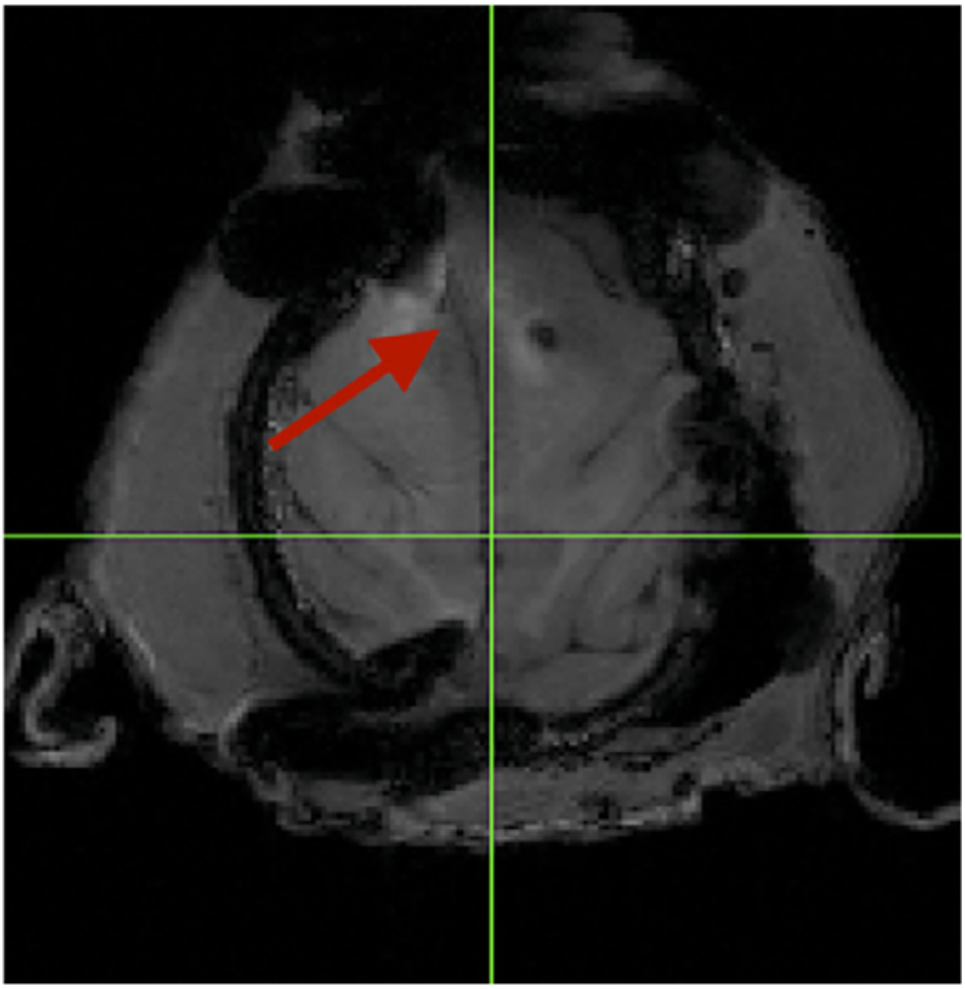

Fig. 6.

Distortion from a titanium implant and screws that are centered over the frontal bone in a NHP. Note the deviation of the midline from center (arrow) as well as the signal voids (black spots) caused by the titanium in the magnetic field during a T1 MPRAGE image acquisition.

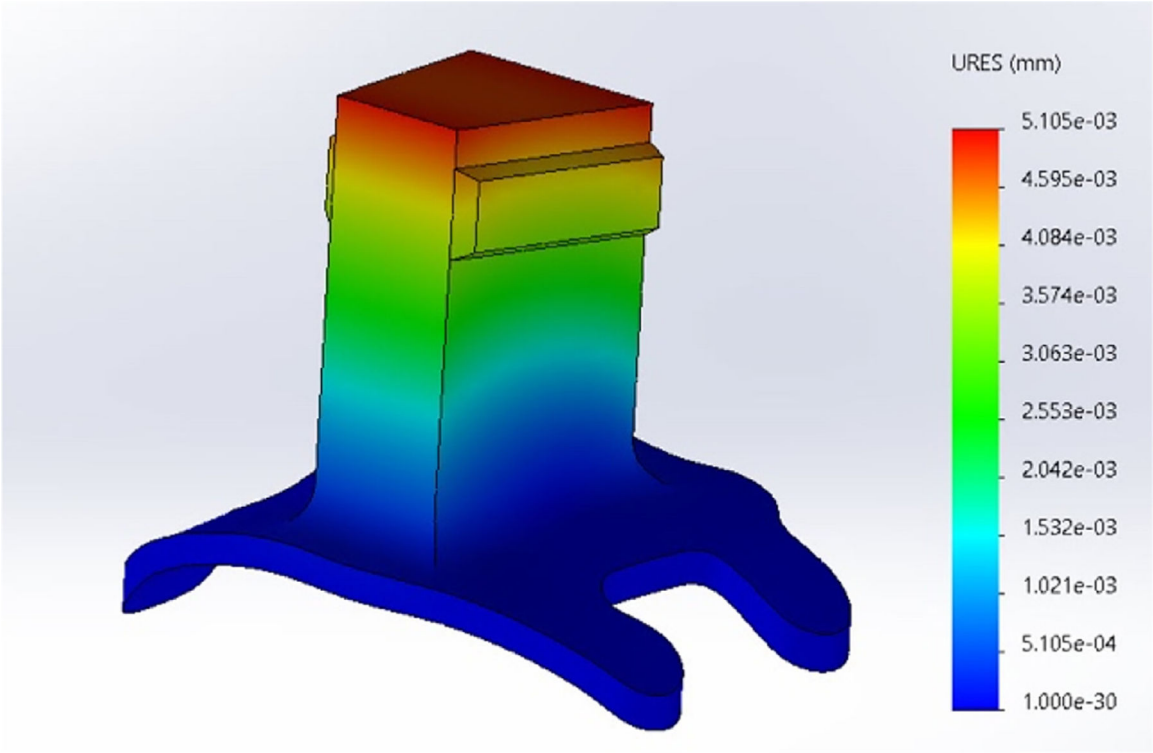

Fig. 7.

In the case of custom designed shapes, simulated stress testing can be done with standard CAD software to judge the strength of a given design.

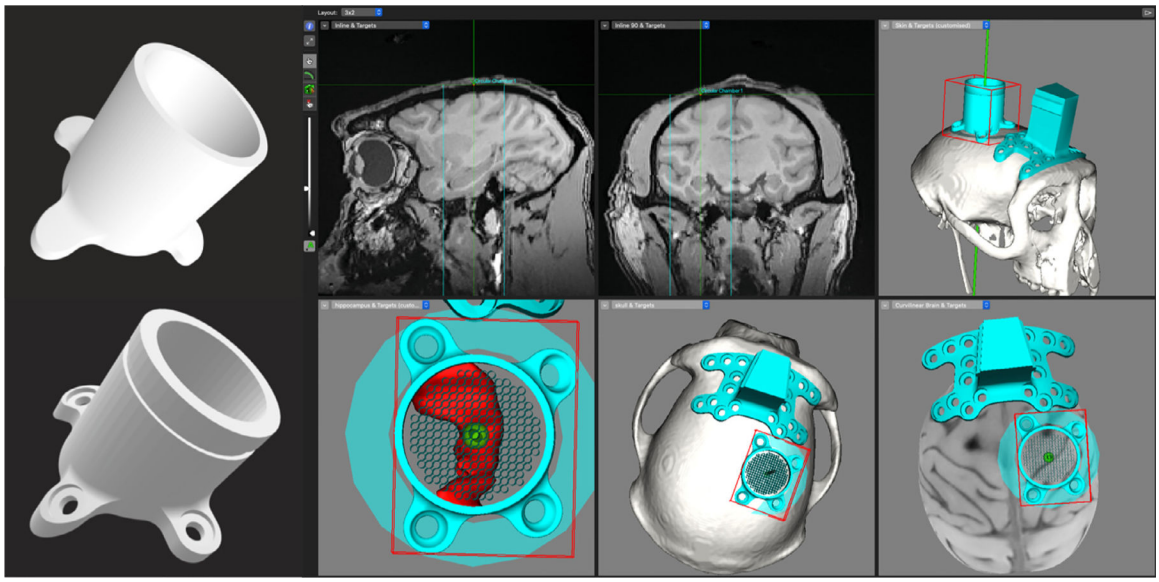

Fig. 8.

CAD files are superimposed on 3D reconstructed skull models and the intersection of the two images are used to generate new CAD files. The CAD files can then be used to create the parts on a 3D printer or manufactured on a CNC machine for higher precision. Pictured above is a custom chamber that is designed to sit over the hippocampus (in red).

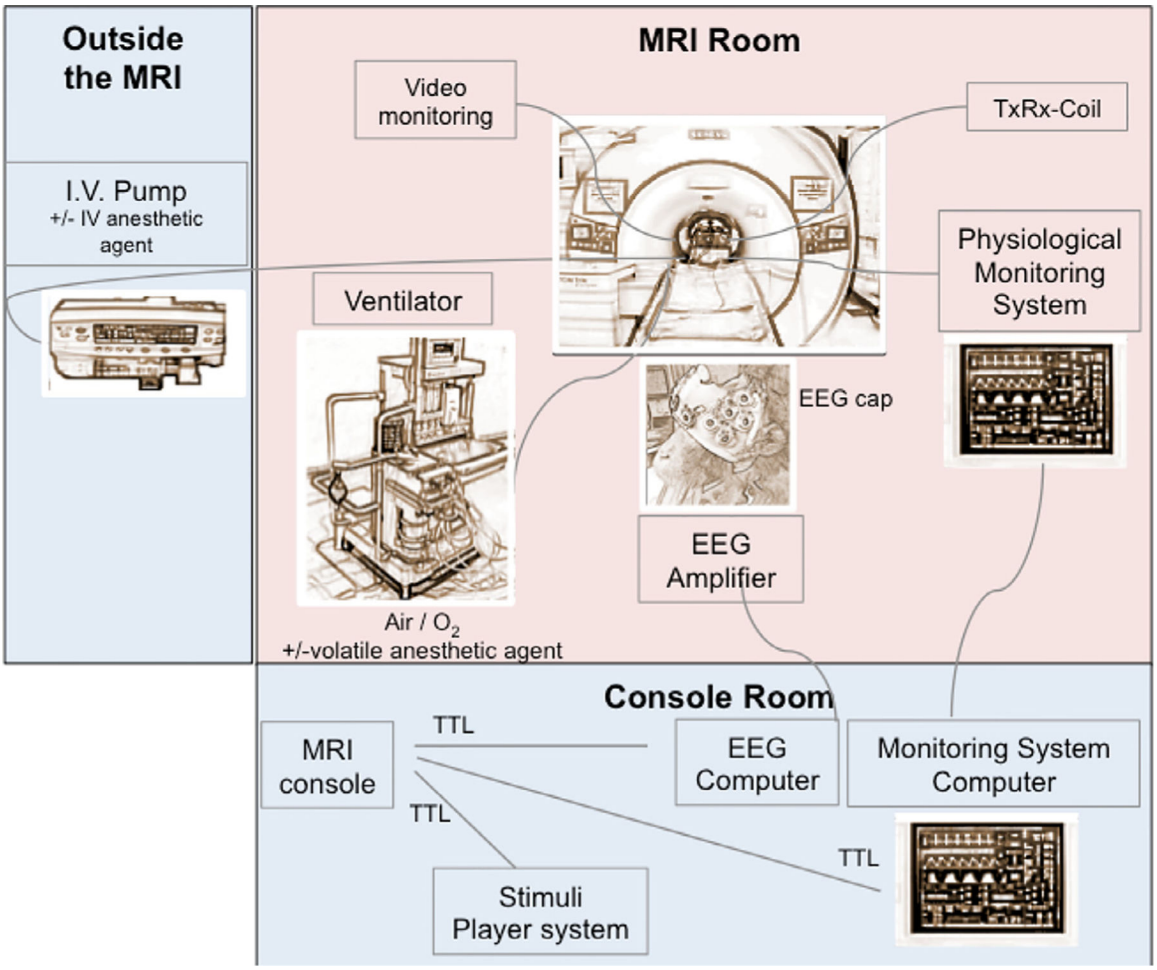

Fig. 9.

Example of an experimental set-up for the anesthesia fMRI studies using a 3T MRI scanner: Representation of an EEG-fMRI set-up for anesthesia experiments in macaques. Red, MRI room with MR compatible devices around the monkey; blue, non-MR devices connected to the MRI room through the wall. TTL, transistor-transistor logic; TxRx, transmit/receive head coil. For this MR compatible anesthesia set-up, most of the material and equipment used (ventilator, physiology monitor, EEG system) match the human clinical regulations, and are commercially available.

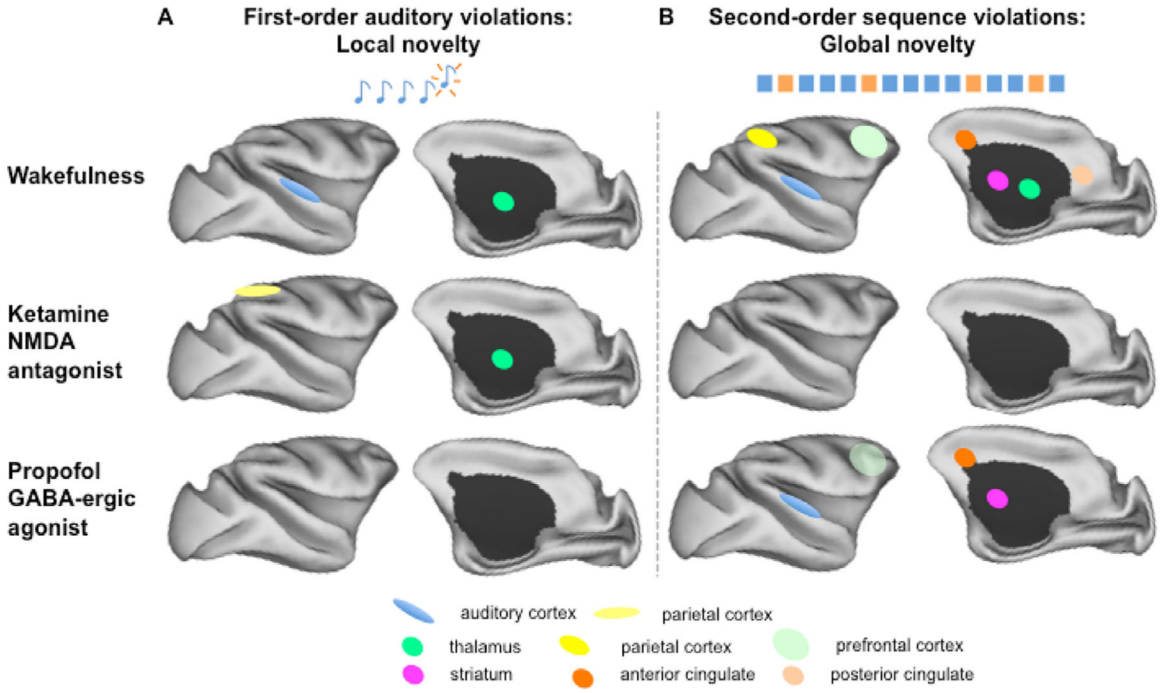

Fig. 10.

Schematic representation of the cerebral activations in the macaque cerebral cortex for the auditory "local-global" paradigm in the awake state and under anesthesia (ketamine, propofol) (Uhrig et al., 2016). A: First-order auditory violations (local novelty effect) in the awake state and under ketamine and propofol anesthesia: The local effect is shifted during ketamine anesthesia compared to the parietal cortex and disappears during propofol anesthesia. B: Second-order sequence violations (global novelty effect) in the awake state and under ketamine and propofol anesthesia: Complete suppression of the global effect under ketamine and disorganization of the global effect under propofol anesthesia.

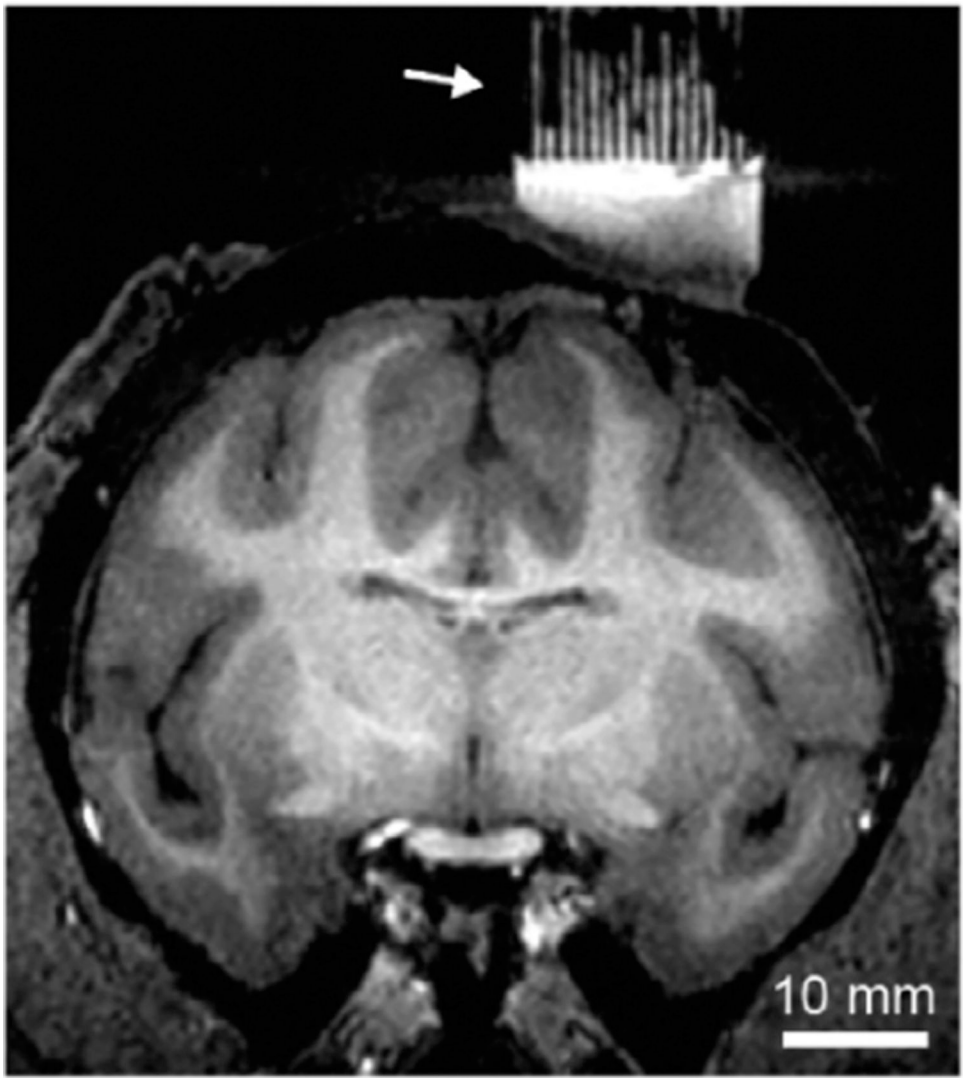

Fig. 11.
MRI with liquid-filled grid (arrow) indicates penetration trajectories into the brain. Image courtesy of Dr. Aidan Murphy.

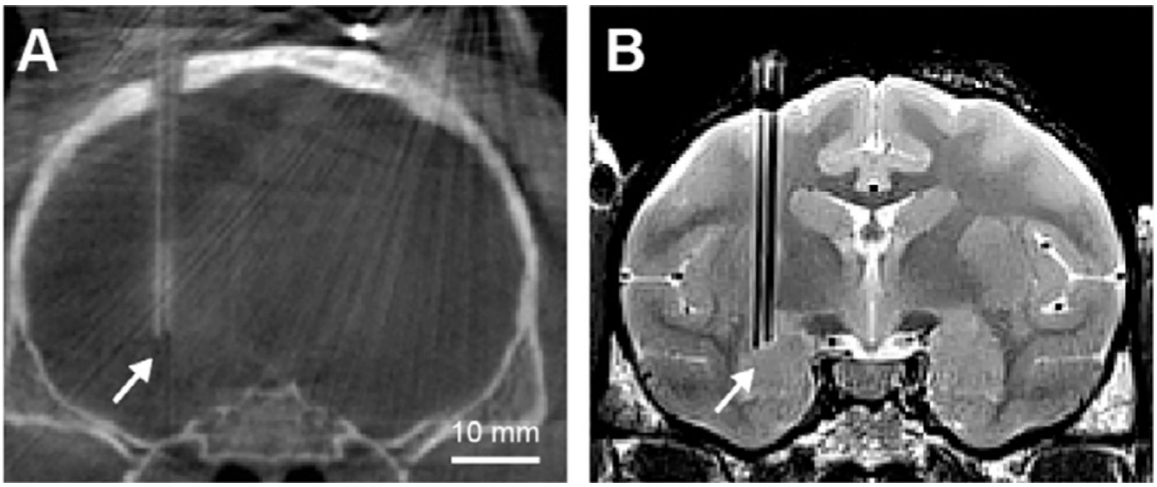

Fig. 12.
A CT and B MR images showing inserted electrodes in the brain.

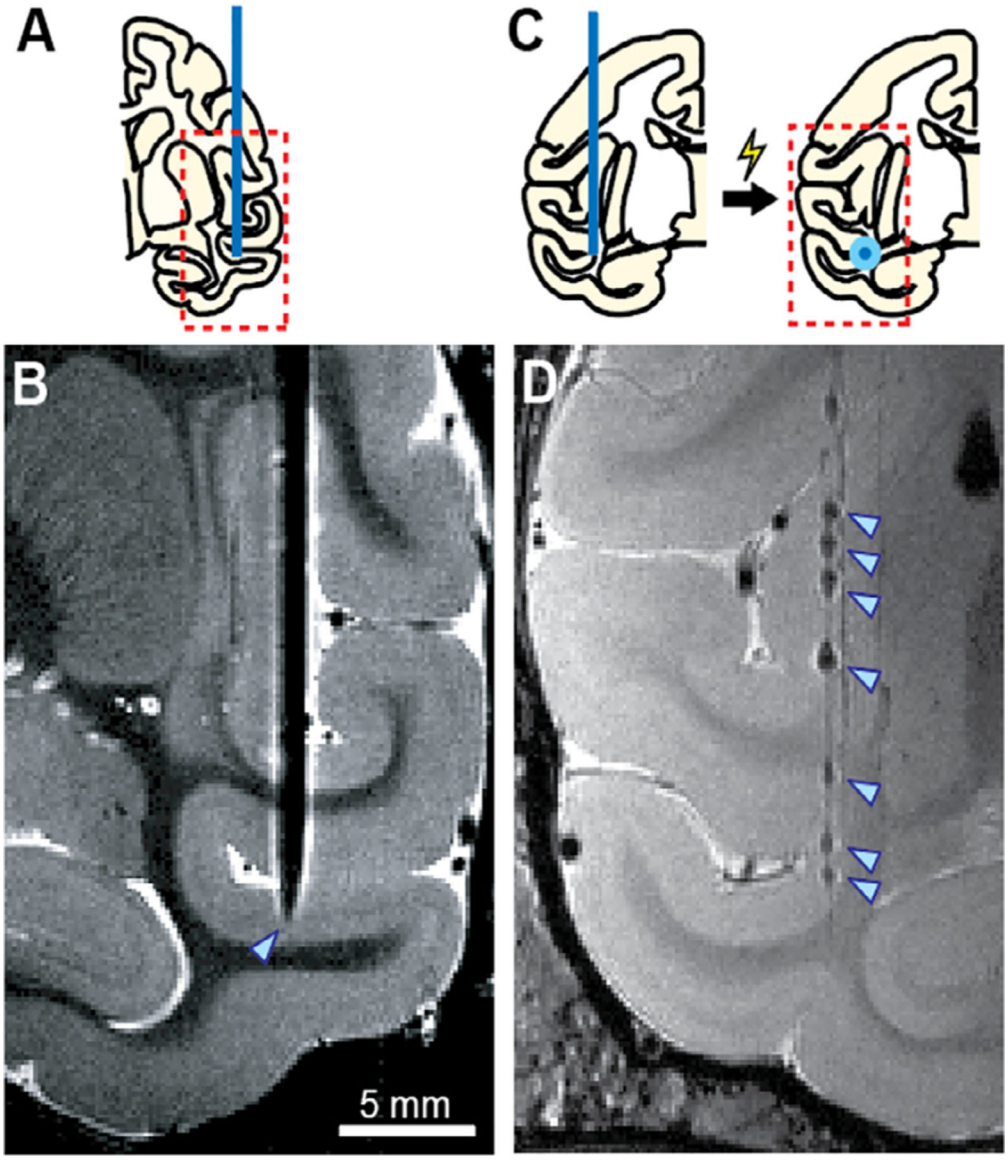

Fig. 13.

MRI-based localization by directly visualizing inserted electrode A, B and marking recording sites with metal deposition C, D. Adapted from Matsui et al. (2007) and Koyano et al. (2011) with modification.

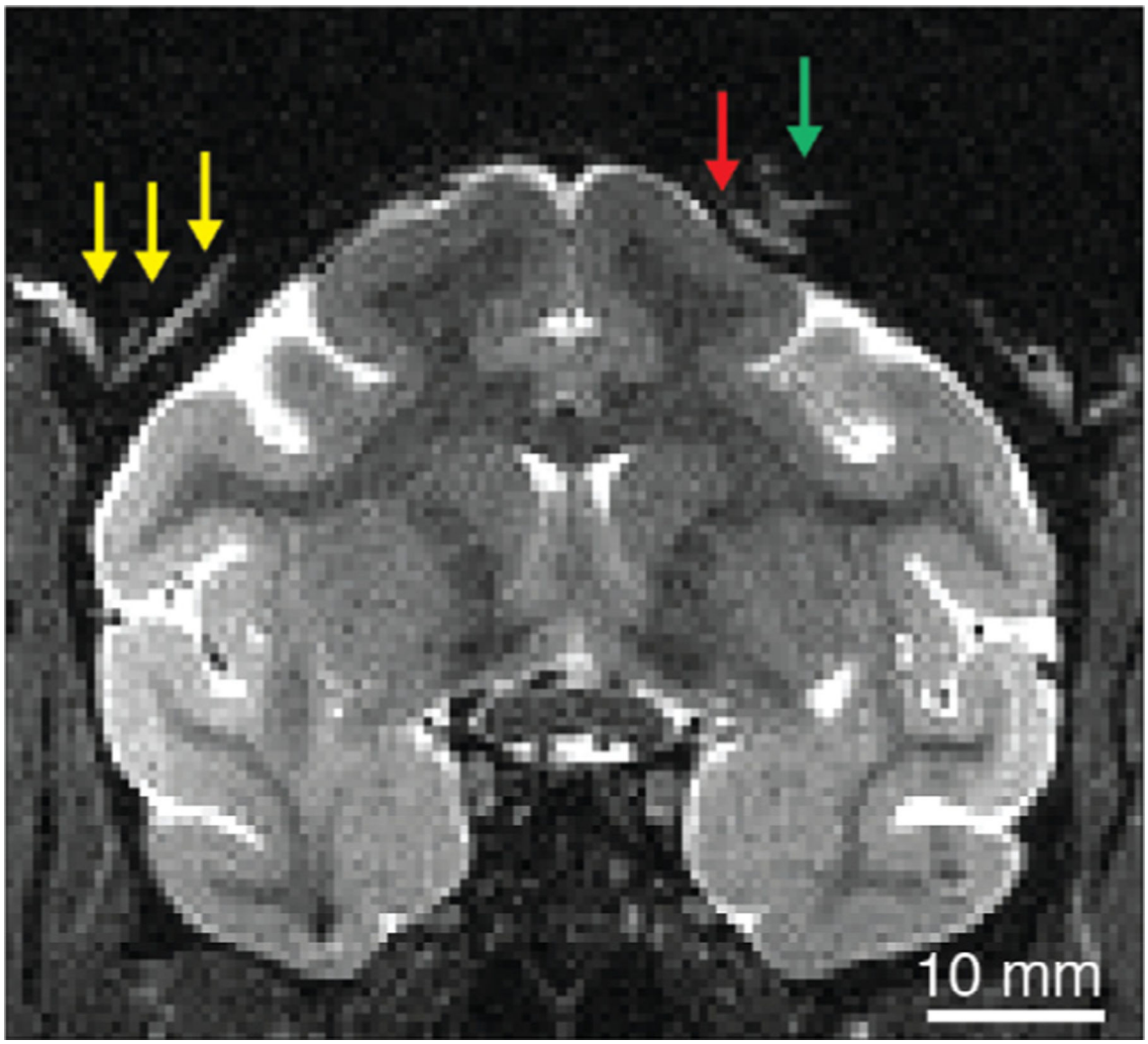

Fig. 14.

T2-weighted anatomical MRI of macaque containing examples of two types of extracranial tissue growth that can be identified early through routine anatomical scans. On the left, light tissue (yellow arrows) has appeared between the skull and overlying acrylic, both of which appear as black. On the right, tissue or fluid from outside the skull (green arrow) communicates with the intracranial epidural space (red arrow). T2 weighted image acquired with fast spin echo (FSE) or rapid acquisition with relaxation enhancement (RARE) sequence.

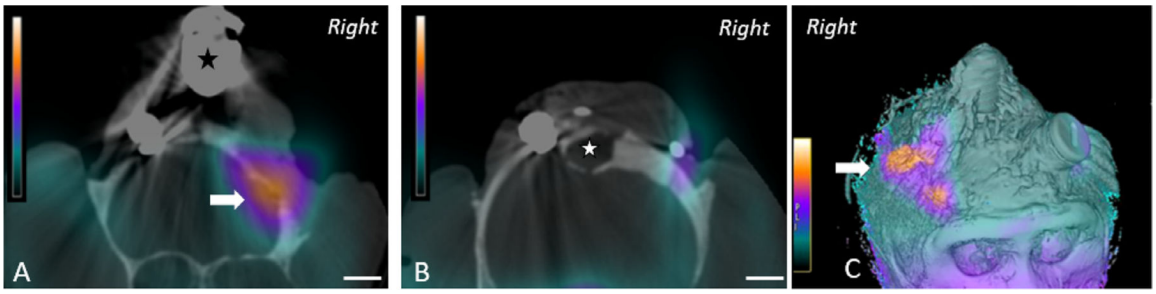

Fig. 15.

SPECT-CT images of the cranium from a rhesus macaque with a long-standing cranial implant. A. Coronal slice of SPECT-CT image just anterior and B. posterior to head post (asterisk), and C. composite image showing strong SPECT signal (arrow) corresponding to exudate beneath the implant (Reprinted with permission from Guerriero et al, 2019).

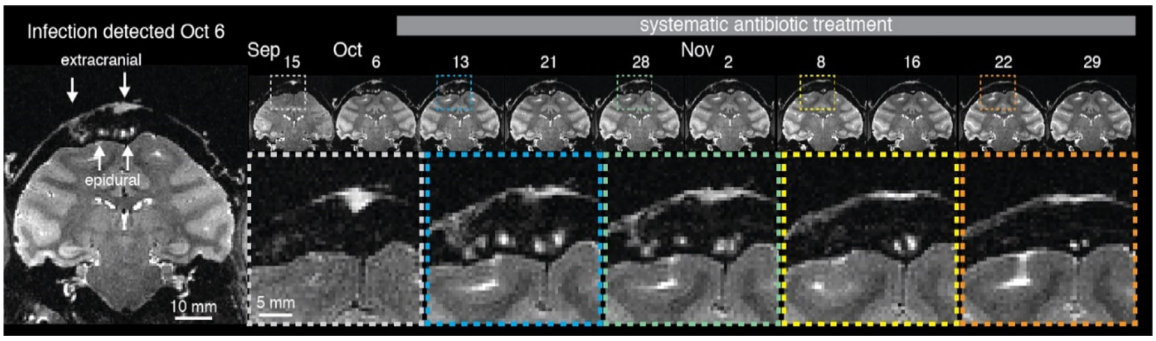

Fig. 16.

Extracranial infection communicating with epidural space detected using routine MRI scan. Systemic antibiotic treatment (TMS + CTX) was initiated on the day of detection. The infection was tracked over the next week and was much reduced in time for a corrective surgery carried out on Dec. 6. T2 weighted image acquired with fast spin echo (FSE) or rapid acquisition with relaxation enhancement (RARE) sequence.

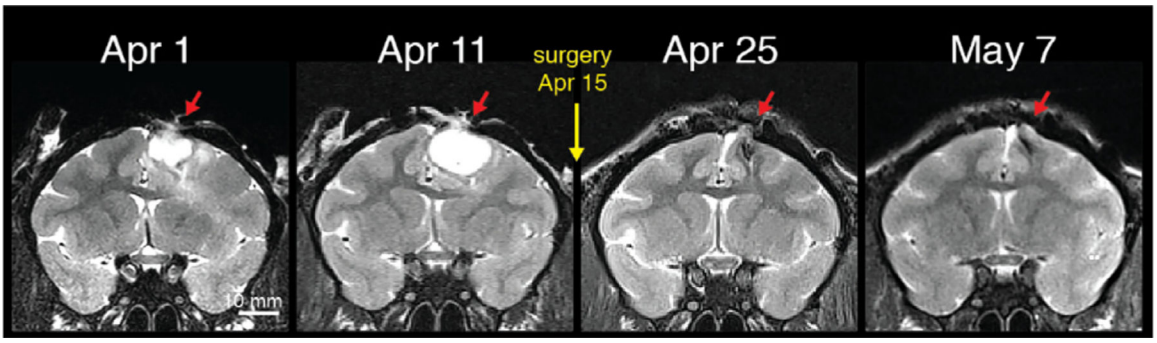

Fig. 17.

A large abscess was detected on Apr. 1 and was treated immediately with systemic antibiotics. A subsequent scan 10 days later demonstrated that the antibiotic treatment was ineffective, as the abscess volume increased. Following the second scan, an emergency surgery was performed, in which the abscess was drained and the implant completely removed. Subsequent scanning demonstrated a complete clearing of the intracranial infection, with scar tissue visible at the previous site of the abscess. T2 weighted image acquired with fast spin echo (FSE) or rapid acquisition with relaxation enhancement (RARE) sequence.

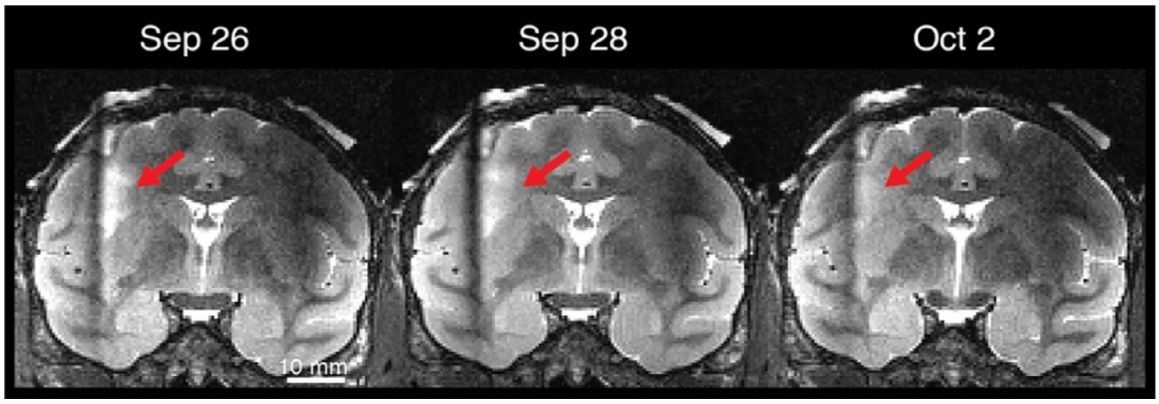

Fig. 18.

Example of large zone of edema in the white matter detected during a routine scan on Sep 26, in association with a chronically implanted deep electrode and prior to overt clinical symptoms. Upon detection, the patient was treated immediately with systemic antibiotics (chloramphenicol and doxycycline), which were effective at treating the infection. T2 weighted image acquired with fast spin echo (FSE) or rapid acquisition with relaxation enhancement (RARE) sequence.

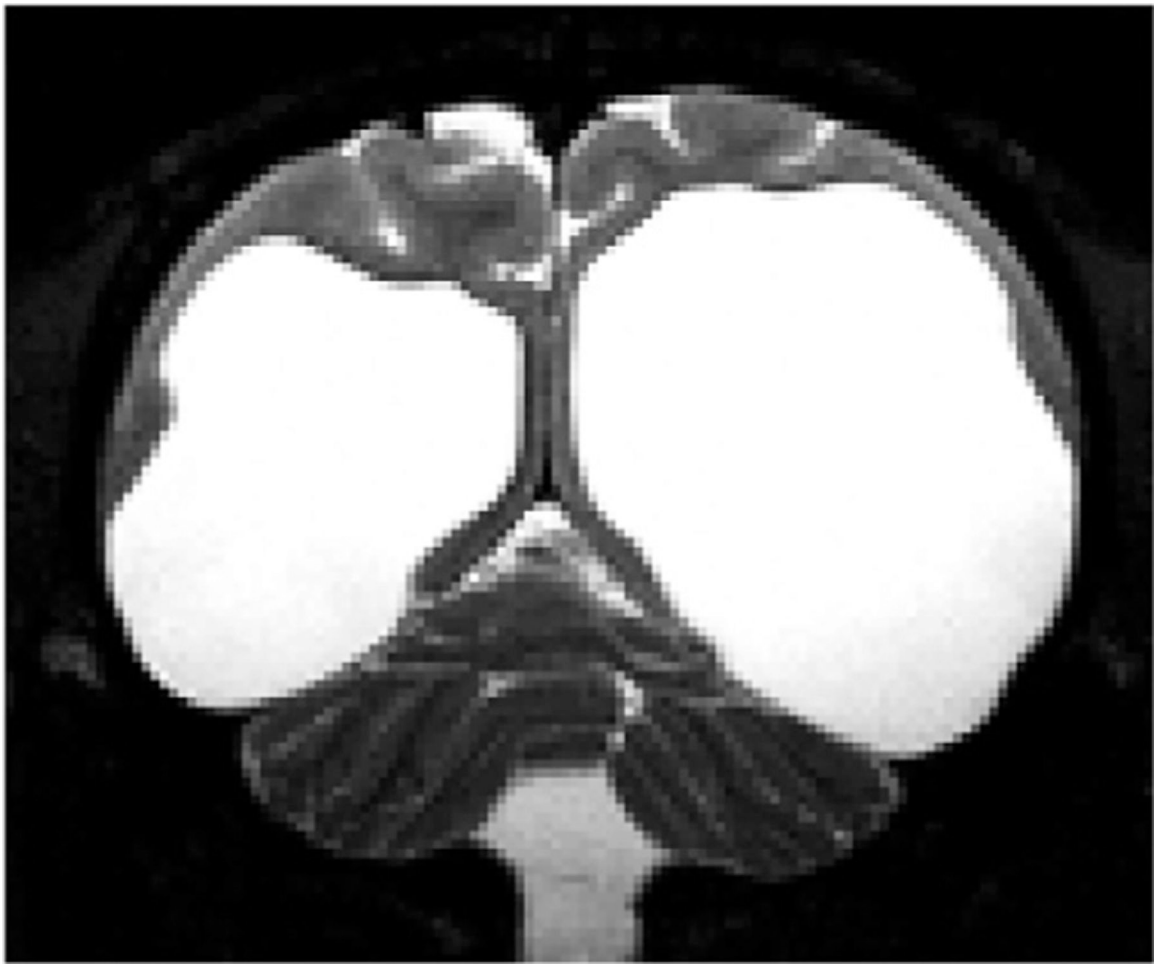

Fig. 19.
Example of an incidental finding from an anatomical scanning session in a macaque. T2 weighted image acquired with fast spin echo (FSE) or rapid acquisition with relaxation enhancement (RARE) sequence.